PATIENT DOSE ASSESSMENT OF ADULT AND PAEDIATRIC CHEST COMPUTED TOMOGRAPHY EXAMINATION: COMPARISON BETWEEN AUTOMATIC EXPOSURE CONTROL AND FIXED TUBE TECHNIQUES.

This thesis is submitted to the:

DEPARTMENT OF MEDICAL PHYSICS SCHOOL OF NUCLEAR AND ALLIED SCIENCES UNIVERSITY OF GHANA, LEGON

BY

CHRISTOPHER K. AGORSAH

(10598858)

In partial fulfilment of the requirement for the award of

MASTER OF PHILOSOPHY

IN

MEDICAL PHYSICS

JULY, 2018

DECLARATION

This thesis is the result of research work undertaken by Christopher Kwasi Agorsah in the Department of Medical Physics, University of Ghana, under the supervision of Prof. Cyril Schandorf, Dr. Stephen Inkoom and Dr. Nii Boye Hammond.

No part of this work has been presented in part or whole to any other university or institution for the award of a diploma, or degree at any level. Other works and/or researches cited in this work have been acknowledged under references accordingly.

……	…….
Christopher Kwasi Agorsah	Dr. Stephen Inkoom
(Student)	(Principal Supervisor)
Date……	Date……
……	…….
Prof. Cyril Schandorf	Dr. Nii Boye Hammond
(Co-Supervisor)	(Co-Supervisor)
Date……	Date……

ABSTRACT

This study was to examine procedures used to estimate radiation dose delivered to adult and paediatric patients undergoing computed tomography (CT) examination and propose alternative and more efficient ways to establish body CT protocols for optimum protection of patient for clinical use. Automatic exposure control (AEC) and fixed tube current (FTC) techniques were used for Polymethylmethacrylate (PMMA) dosimetry phantoms in a Siemens emotion 16-slice multidetector computed tomography (MDCT) scanner. Chest CT scan was simulated for adult and paediatric patients using CT-Expo software and dose measurements using RTI barracuda system with electrometer and CT dose Profiler probe. Estimates of effective doses to the chest were done based on ICRP publication 103 recommendations and doses to organs at risk in the chest were estimated using CT-Expo software. It was observed that measured absorbed doses for adult chest examinations deviated from the console values by 1.71 and 10.50%, and that for paediatrics deviated by -68.83 and -52.83% for $CTDI_{vol}$ and DLP respectively. Statistical analysis demonstrated a highly significant correlation between measured and console CTDI values of $P < 0.001$. Simulated doses for adults deviated from the console values by 23.40 and -34.44%, whiles that for paediatrics deviated by -59.47 and -91.55% for $CTDI_{vol}$ and DLP respectively, showing that radiation dose delivered to patients may not always be the same as that displayed by the CT console and would not be reliable in dose estimation and safe scan protocols. Measurement of radiation dose output of a CT scanner would require the right phantom size in order to obtain safe values consistent with good image quality. Also, dose reduction for the adult and paediatric chest examinations were -4.96 and 38.80 % respectively, between AEC and FTC techniques for both CTDI values showing that even

though the paediatric doses were relatively high compared to other studies, there was appreciable dose reduction with the AEC technique. AEC has therefore proven its dose reduction efficacy and has the advantage of providing a more generalized but focused approach that might be relevant to use among paediatrics and small adults. Meanwhile, activation of the AEC in the adult chest CT examination resulted in an increase in radiation dose of 4.96% between the AEC and FTC techniques. The use FTC has therefore shown some level of dose reduction capability that could be used to optimize dose for adults and large patients. In conclusion, both AEC and FTC techniques can be employed in the optimization of chest CT examinations and should be incorporated in the establishment of chest CT protocols with respect to patient body size and according to the clinical task. This emphasises the need for medical physicists and radiographers to seriously consider the use of AEC and FTC as dose reduction techniques for patient radiation protection. There is the need to continue to re-examine and refine CT scan procedures for the optimization of patient protection.

DEDICATION

I dedicate this work to my parents for their care and endless support throughout my life. Specifically, I dedicate the study to Dr. E. Kofi Agorsah, Professor Emeritus, who has been my father and backbone support throughout my studies, and to my two brothers, David Agorsah and Isaac Agorsah and to my entire family, friends and loved ones.

ACKNOWLEDGEMENTS

I am very grateful to my very highly dedicated supervisors Prof. Cyril Schandorf, Dr. Stephen Inkoom and Dr. Nii Boye Hammond for their guidance, encouragement and educative comments and unflinching support during the entire research process. I am deeply indebted to them, as well as, to all my technical support staff and lecturers and supervisors for their encouragement, criticisms, motivation and for being there for me especially during the most trying moments. I sincerely share the credit of this work with them all.

My heartfelt gratitude goes to Mr. Philip Oppong Kyereme Jnr., Mr Dormenyo D. Gadeka and Mr. George Felix Acquah of the Sweden-Ghana Medical Centre (SGMC) for making a large amount of data and support material available to me for the study. I will carry memory of their hard work, dedication and patience with me and especially for always readily assisting and providing all needed materials for this research. A special appreciation goes to Dr. Shirazu Issahaku, whose guidance in fine-tuning and making the write-up of the study clearer and presentable. There are many more to mention but it is impossible to list all the many friends, colleagues and family, who have supported me. Finally, my greatest thanks goes to the Department of Medical Physics, School of Nuclear and Allied Sciences, University of Ghana, for the opportunity and experience of a life time and promise to carry along the banner and the good name of the institution.

TABLE OF CONTENTS

LIST OF FIGURES

LIST OF TABLES

LIST OF ABBREVIATIONS

AAPM	American Association of Physicists in Medicine
ACR	American College of Radiology
AEC	Automatic Exposure Control
ALARA	As Low As Reasonably Achievable
ASIR	Adaptive Statistical Iterative Reconstruction
ASRT	American Society of Radiologic Technologists
cGy	Centigray
CT	Computed Tomography
CTA	CT angiography
CTDI	CT dose index
$CTDI_{vol}$	Volume CT dose index
$CTDI_{w}$	Weighted average CT dose index
CTDP	CT Dose Profiler Probe
DLP	Dose Length Product
DR	Dose Reduction
EBT	External Beam Radiotherapy
ED	Effective Dose
FBP	Filtered Back Projection
FDA	U.S Food And Drugs Administration
FOV	Field Of View
FTC	Fixed Tube Current
Gy	Gray
ICRP	International Commission on Radiological Protection
IR	Iterative Reconstruction

IRAs	Iterative Reconstruction Algorithms
IRIS	Recent Reconstruction In Image Space
kV	Kilo Voltage
kVp	Kilo voltage peak
mAs	Current (mA) multiplied by time (seconds)
MBIR	Model-Based Iterative Reconstruction
MCDA	Multiple Computed Detector Arrays
MDCT	Multi-Detector Computed Tomography
mGy	Milligray
MSAD	Multiple Scan Average Dose
MSCT	Multi-Slice Computed Tomography
mSv	milliSieverts
MV	Mega Voltage
NRA	Nuclear Regulatory Authority
PET	Positron Emission Tomography
PMMA	Polymethyl Methacrylate
RSNA	Radiological Society of North America
SGMC	Sweden Ghana Medical Centre
SNR	Signal-to-Noise Ratio
SPECT	Single Photon Emission Computed Tomography
SPSS	Statistical Package for Social Sciences
UNSCEAR	The United Nations Scientific Committee on the Effects of Atomic Radiation

CHAPTER ONE

1.0 INTRODUCTION

This chapter gives the general background of the research work, the research problem, objectives, justification, scope and organization of the thesis.

1.1 Background

Several developments have taken place in the medical field in the last century and Computed Tomography (CT) is one of the few that have had far-reaching impact on patient diagnosis and inside view of the human and even animal body. Computed Tomography (CT) as a medical diagnostic technique has played a very important role in health care in the last half century and has since then been adopted by many medical institutions, practitioners and manufacturers. Godfrey Hounsfield (1973) was the first to introduce the technique in 1972 and it has since embraced additional advances and clinical advantages in medical diagnosis (Ambrose & Morley, 1973; Hounsfield, 1973). There has been concerns of the harmful effects of using ionizing radiations in radiological examinations. Increase in radiation dose through CT scan may be largely due to over-beaming, positioning of the X-ray tube closer to the patient, significant increase of repeated scan, scan overlap, increased scatter radiation with wider X-ray beams (Mccollough & Zink, 1999). It would be fair, therefore to argue that the possible harmful effect of exposure to ionizing radiation on healthy tissue could be considered a disadvantage and must be minimized.

Dose optimization, for example, is now crucial in clinical routines due to the frequent use of CT examination in medical diagnosis and its associated potential risk factors particularly in cancer patients who are often required to take frequent follow-up CT examinations (Brenner & Hall, 2007; Pearce et al., 1985). The United Nations Scientific Committee on the Effects of Atomic Radiation (UNSCEAR) gave a report on the Medical Radiation Usage and Exposures which showed the contribution of CT to be about 43% of the total radiation dose from diagnostic medical radiology (UNSCEAR, 2008). In 2005-2006, it was estimated that 60% of the total radiation dose from diagnostic radiology was from CT examinations in the United Kingdom (Hall & Brenner, 2008).

Consequently, considerable research on optimization of CT scan protocols have been undertaken in certain developed countries (Kubo et al., 2014; Papadakis et al., 2008; Suess, 2002; Yu et al., 2010). A study by Gedel et al. (2014) in Ghana has shown that exposure parameters used for paediatric CT examinations were similar to those used for adult CT examinations for some hospitals, resulting in increased dose levels delivered particularly to children. The issue of the safe radiation level continues to be debated among medical practitioners and is the rationale of this study.

1.2 Problem Statement and Objectives

The need to arrive at some additional definitive conclusions is one of the main objectives of this project on the optimisation of paediatric and adult CT examination protocols to determine the radiation level(s) that would ensure optimum protection particularly for paediatrics. Overexposure of patients to ionizing radiation is not visually indicated in the

final image in CT as opposed to the conventional screen-film imaging in which the film is darkened. On the other hand, it tends to reduce image noise, a requisite component of the image quality, thereby increasing the possibility of the radiologist overlooking overexposure (Bauhs et al., 2008). The diagnostic advantage of CT has increased the demand for CT examinations worldwide. Taking into consideration the radiation risk associated, it has become crucial to find ways by which one might reduce radiation dose from CT examinations. One of the major challenges in CT clinical practice is the choice of specific combination of optimized CT technique factors that can be used for exact body anatomy to produce images of good diagnostic quality while delivering minimal radiation dose to patients.

Over the years, CT manufacturers have incorporated techniques that alter the acquisition parameters with the aim of reducing radiation dose level delivered to patients. Modern CT scanners have introduced automatic exposure control (AEC) systems that adapt the tube current (mA) to conform to the attenuation variations within the patient based on user-defined adjustments for different spatial projections or at specified times. The aim was to produce images of good diagnostic quality at reduced patient doses (Sookpeng et al., 2013). It is imperative to evaluate the influence of exposure parameters on the dose delivered to children and adult patients and the image quality. The objective of this study was to determine optimised CT scan protocols for both adult and paediatric patients undergoing chest CT examination.

1.3 Specific Objectives

This research work seeks to examine radiation doses delivered to patients when AEC and FTC techniques are used leading to the establishment of optimal chest CT protocols for adequate protection of the adult and paediatric patients offered by the 16 slice Siemens CT scanner used at the radiology department of the Sweden Ghana Medical Centre (SGMC), located in Accra, Ghana. Specific objectives include;

- To use PMMA dosimetry phantoms to examine patient doses when Chest examinations are done using AEC and FTC techniques for adult and paediatric patients.
- To evaluate the effect of AEC on dose reduction.
- To intercompare measured, simulated and CT console doses.
- To explore options for dose optimisation
- To make appropriate recommendations based on findings of the study.

1.4 Justification

Depending on the clinical need, CT examination may not be equally replaced by other low radiation or radiation-free imaging modalities mainly due to its clinical benefit and advantage. For instance, CT images serve as the basis in radiotherapy treatment planning for cancer. CT has good contrast, which enables imaging of soft tissues and bony structures due to its great spatial resolution. Even with these benefits, dose reduction continues to be elusive but crucial as the technology advances and the demand for quality CT scan increases. Certain CT manufacturers have incorporated techniques that alter the

acquisition parameters geared towards the reduction of radiation dose to patients. Prominent among them is the AEC system, which adapts the tube current (mA) to account for attenuation variations within the patient based on user-defined adjustments for different spatial projections or at specified times. However, a major drawback of this technique is that radiation dose delivered to larger patients may be increased (Keat, 2005). It is, therefore, important to determine the influence the primary scanning parameters have on the dose delivered to the patients and the diagnostic relevance of the image quality. The findings will help reduce radiation dose from chest CT examinations especially in paediatric patients; this will subsequently lower potential radiation risks particularly with cancer patient and patients suffering from chronic diseases who require frequent follow-up examinations. Results will also contribute substantial information to the body of knowledge on the subject matter among the scientific community.

1.5 Scope and Organization of the thesis

The study was carried out using a 16 slice Siemens CT scanner at SGMC radiology department. The effect of tube current on patient dose was assessed by comparing AEC with fixed tube current (FTC) techniques. Effective and organ doses were estimated for each of the techniques for paediatric and adult chest CT examinations using PMMA dosimetry head (16 cm diameter) and body (32 cm diameter) phantoms respectively. The thesis is made up of five chapters with the first chapter as an introduction to the research giving the background of the thesis, statement of problem of study, objectives, relevance and justification and scope of the thesis. Chapter two focuses on the current literature available and reviews some recent advances in the field that are relevant to the study. The

materials and experimental framework and the method of approach and techniques are presented in the third chapter. Chapter four presents the results obtained and relevant discussions. Chapter five provides conclusions on the major findings and recommendations to some key stakeholders.

CHAPTER TWO

2.0 LITERATURE REVIEW

This chapter presents a general overview of the principles of computed tomography and the evolution of CT scanners over the past years. It analyses the various advances in techniques used by various CT manufacturers and users in dose reduction. The influence of the use of tube current (mA) and kilo voltage peak (kVp) on dose reduction and image quality and their implications are discussed to prepare the way for examining possibilities for needed improvement(s).

2.1 Introduction

CT has evolved considerably since its introduction in the 1970s (Hounsfield, 1973). It was the most modern imaging machine following the X-ray machine at the time and was popularly known as the "computed axial tomography" due to its ability to produce non-superimposed, cross-sectional images of the body. The cross-sectional display is advantageous as it gives an improved visualization into the pathogenesis of the anatomy under study. It has been an alternative to other imaging modalities such as magnetic resonance imaging and ultrasound that are imperfect in demonstrating anatomical and pathological structures for accurate diagnosis (Livingstone et al., 2010).

Use of CT has risen and continues to rise since its introduction, probably due to advancement in the technology and innovations in the imaging field. CT has become a popular imaging modality used to provide patients with detailed anatomical information and an indispensable diagnostic tool. CT can be fused with other imaging modalities by

merging the results of different types of examinations. For example, CT fuses with functional imaging such as Positron Emission Tomography (PET) and Single Photon Emission Computed Tomography (SPECT) by merging results of different kinds of examinations. This helps radiologist and other physicians in making more accurate diagnosis since the image provides anatomic detail coupled with functional information in this case. All these help improve patient health care.

Later, CT scanners evolved from single slice axial to helical and multi-slice models. In the early stages, the CT scanner used a single detector, which rotated 360 degrees or less with a stationary patient table making it possible to take one image at a time (Cunningham et al., 2000). Since 1990, CT was recognised as one of the most beneficial imaging modality after the introduction of multi-slice scanning with the advantage of higher patient comfort - lower sedation for paediatrics and fewer breath-holds in body imaging (Zenger, 2015). Thinner sections and shorter examination time has also been achieved and this has increased use of CT examinations in emergency departments and as a substitute to other imaging modalities (Weber, 2001). The technology then developed from units ranging from 4 up to 640 slices and expanded anatomical coverage making scanners even faster and portable and referred to as "Multi-Slice Computed Tomography (MSCT)" or "Multi-Detector Computed Tomography (MDCT)".

The frequency of CT examination continues to rise and public awareness has also risen, such that radiation dose reduction has become a critical issue in CT examination practices due to high radiation dose delivered to patients. Many scholars have emphasized the need to put some measures in place to keep the radiation exposure as low as possible and to improve diagnostic image quality (Jurik et al., 1997). A major requirement of any

exposure is the proper justification of the procedure which takes into account the radiation protection of the subject under consideration (Catalano et al., 2007). This is in compliance with the recommendations of the International Commission on Radiological Protection (ICRP). Once a CT examination is clinically acceptable then it should be justified and optimized. It is the responsibility of CT manufacturers, medical physicists and radiologists to make a collective effort towards developing CT scanners and practicing optimization of scan protocols aimed at reducing patient dose from CT examinations (Kalra et al., 2004).

Radiation dose can be optimised in two major ways: the first is through the design of the equipment and the second is optimization of the scan protocols (Lewis & Edyvean, 2005). Recent advances also indicate that image quality has several components and is affected by many technical parameters used in the CT examination. These same parameters are those adjusted in order to deliver minimum dose to patients while obtaining clinically acceptable image quality. Radiation dose reduction can be achieved by means of improved hardware techniques such as use of sliding collimator to eliminate unnecessary radiation exposure to critical or healthy organs as well as following various principles such as use of tube current modulation, minimizing scan length, minimizing tube current, minimizing tube potential, tailoring a scan to a patient and Iterative Reconstruction (IR) among others. A study by Siegel et al. (2004) showed that it is possible to reduce radiation dose in paediatric contrast-enhanced CT examinations by reducing tube current and tube potential at acceptable diagnostic image quality. Mathematical post-processing algorithms are also used to reconstruct the images at reduced image noise levels. The conventional Filtered Back Projection (FBP) reconstruction algorithm has some level of quantum noise which can be minimised using IR algorithms such as; iDose (Philips), Model-Based Iterative

Reconstruction (MBIR; GE Healthcare), Recent Reconstruction In Image Space (IRIS; Siemens), Adaptive Statistical Iterative Reconstruction (ASIR; GE Healthcare) and many more (Ghetti et al., 2012). However, a major drawback of these image domain-based Iterative Reconstruction Algorithms (IRAs) is a modification of the visual appearance of images making them to appear smooth (IRIS) or pixelated (ASIR) rendering the images less clinically informative. Each vendor adopts a unique iterative reconstruction technique used to manipulate the outcome of the image quality, which may include noise reduction, contrast enhancement, increase in Signal-to-Noise Ratio (SNR), etc.

CT dose is usually quantified using certain dose descriptors chosen for dose estimation. The principal dosimetry quantity is the CT dose index (CTDI) and is used to describe the X-ray tube radiation output of the scanner. Volume CT dose index ($CTDI_{vol}$) measurements can be made at the core and periphery of the head and body CT phantoms with the aid of ionization chambers and other detectors. The body PMMA dosimetry phantom is used to represent the adult body whereas the head PMMA dosimetry phantom is used to represent the paediatric body by some manufacturers. Weighted average CT dose index ($CTDI_w$) is obtained by a combination of the dose values measured which is an estimate of radiation dose delivered to the phantom.

The American Association of Physicists in Medicine (AAPM) is one of the professional groups that have championed the standardization of clinical practices that employ use of CT in medical diagnosis (Trattner et al., 2014). The goal has been to deliver the lowest dose to patients while obtaining the diagnostic image quality. It is not ideal to use the same CT acquisition and reconstruction parameters for all patients due to variation in patient anatomy and attenuation properties. Reduction of dose can, therefore, be

achieved by selecting the optimal CT technique factors following patient-centred examination practices. It would be desirable to re-examine some of these advances and to propose additional measures that could reduce radiation dose while enhancing image quality.

The campaign for Image enhancement has also been a priority in recent years for the American College of Radiology (ACR) and the Radiological Society of North America (RSNA) in collaboration with the American Society of Radiologic Technologists (ASRT) and AAPM. The aim of this campaign has been to publicise the precise clinical indications of adults medical imaging examinations in order to optimize radiation dose (Butler et al., 2016; Hossain, 2015). The hope has been to advance safe and effective imaging care, particularly of children, globally through advocacy. Despite these advances, the challenges remain and should provide platforms for some of the considerations of this study by firstly considering some related basic principles, some of which are discussed in the section that follow.

2.2 Principles of Computed Tomography (CT) Operation

There are basically two phases involved in obtaining a CT image. First, X-rays are transmitted through a patient and the attenuation of the X-rays traversing the patient at different projection angles is measured. Taking a third generation CT scanners, described later as an example for the data acquisition process, the X-ray tube and the detector array situated at opposite sides of the patient rotate around the patient (Cunningham et al., 2000). The X-ray tube and detector geometry has evolved over the past years. The various

geometries are described in the generations of CT scanners below. The attenuation is dependent on the energy of the X-rays and also on the patient's average atomic number and mass density (Cunningham et al., 2000). The second phase has to do with mathematical calculations of the linear attenuation coefficients, μ, over the entire slice. The intensity of the transmitted beam is given by:

$$I_t = I_0 e^{-\int_0^L \mu(x)dx} \tag{2.1}$$

where I_o and I_t represent the incident and transmitted beam intensities, respectively; L is the X-ray path length; and μ(x) is the X-ray linear attenuation coefficient, that varies with tissue type (Cunningham et al., 2000). The integral of the attenuation coefficient is also given as:

$$\int_0^L \mu(x)dx = \frac{1}{L}\ln(I_t / I_0) \tag{2.2}$$

Readings from each detector are saved in the computer memory after which the X-ray tube is rotated to a different angle for a new projection profile measurement. After a complete rotation, the patient table is moved a small distance determined by the pitch for the next slice measurement. The average linear attenuation coefficient, μ, for each voxel can then be calculated from the data sets of projection profiles given through all voxels in a section of the patient for adequate projections. This operational technique needs some consideration as to how much more improved impact it has on CT results.

2.3 X-ray Production

Another operational procedure relates to how X-rays are produced when electrons accelerated through a high potential difference ranging from 1 kV to 1 MV are made to strike a metal target interacting with its atoms (Zink, 1997). The electrons originate from a heated filament by thermionic emission and are accelerated to hit a target anode shown in Figure 2.1.

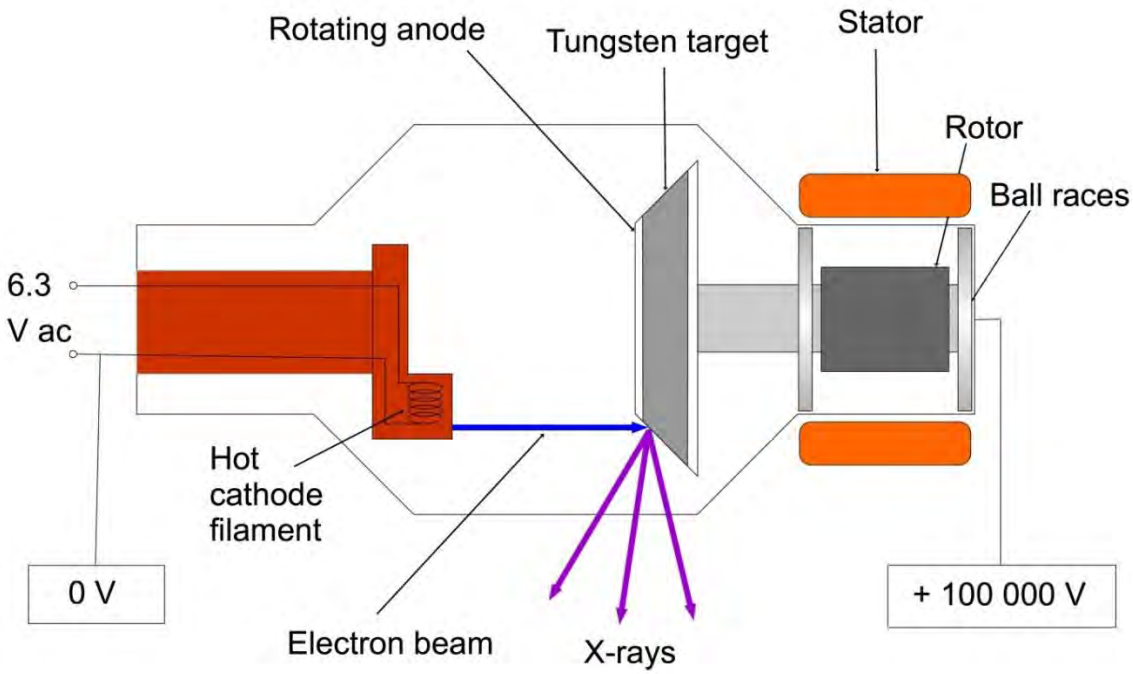

Figure 2. 1: Schematic diagram of the X-ray tube (Zink, 1997)

The filament current constitutes the flow of electrons in the wire filament within the cathode. Likewise, the flow of electrons between the cathode and anode components of the tube is called the tube current. Upon hitting the anode, the electrons are decelerated causing part of the kinetic energy to be converted into electromagnetic energy such as X-rays and

the rest is converted into heat or internal energy of the target. During the breaking down process, the electrons go through a complex sequence of collisions and scattering process which leads to the production of bremsstrahlung and characteristic X-rays (Zink, 1997). An electron may be forced to change its direction by coulomb forces as it comes close to an atomic nucleus causing it to emit electromagnetic radiation known as bremsstrahlung. Figure 2.2 shows a schematic diagram of bremsstrahlung production process.

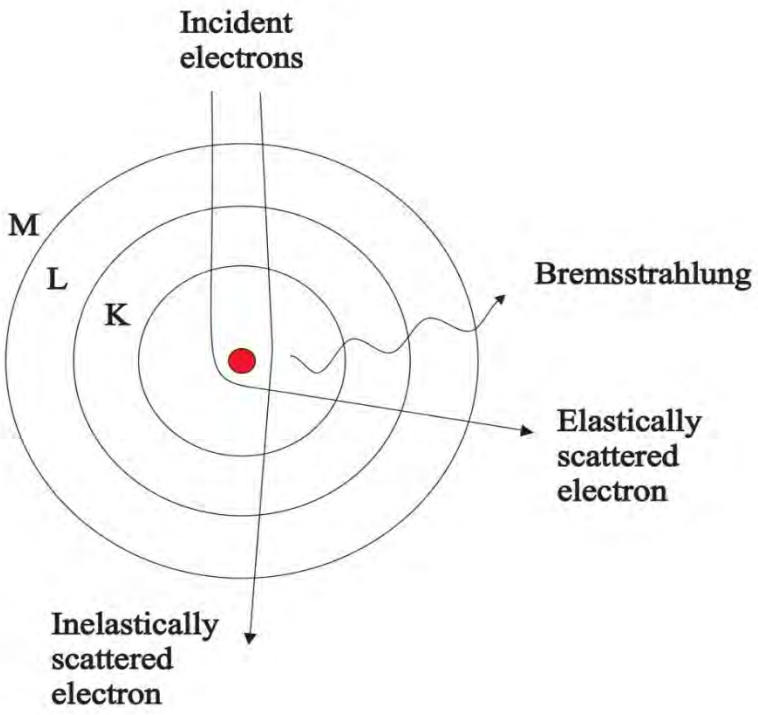

Figure 2. 2: Schematic diagram of bremsstrahlung production process.

The energy of the bremsstrahlung rests on the attractive coulomb forces and the distance of the electron from the nucleus. The kinetic energy of the electrons may vary due to the potential difference not being constant across the tube resulting in an energy spectrum.

Characteristic X-rays may be produced by fast moving electrons as they collide with inner shell electron of an atomic shell knocking it out once its KE exceeds the binding energy of the electron in that shell shown in Figure 2.3. The scattered primary electron goes away with energy equal to the difference between the kinetic and binding energies. When this happens, an electron from an outer shell fills the vacancy by the emission of a characteristic X-ray with energy equal to the difference in binding energies of the shells involved. These X-rays are characteristic of the element used for the production.

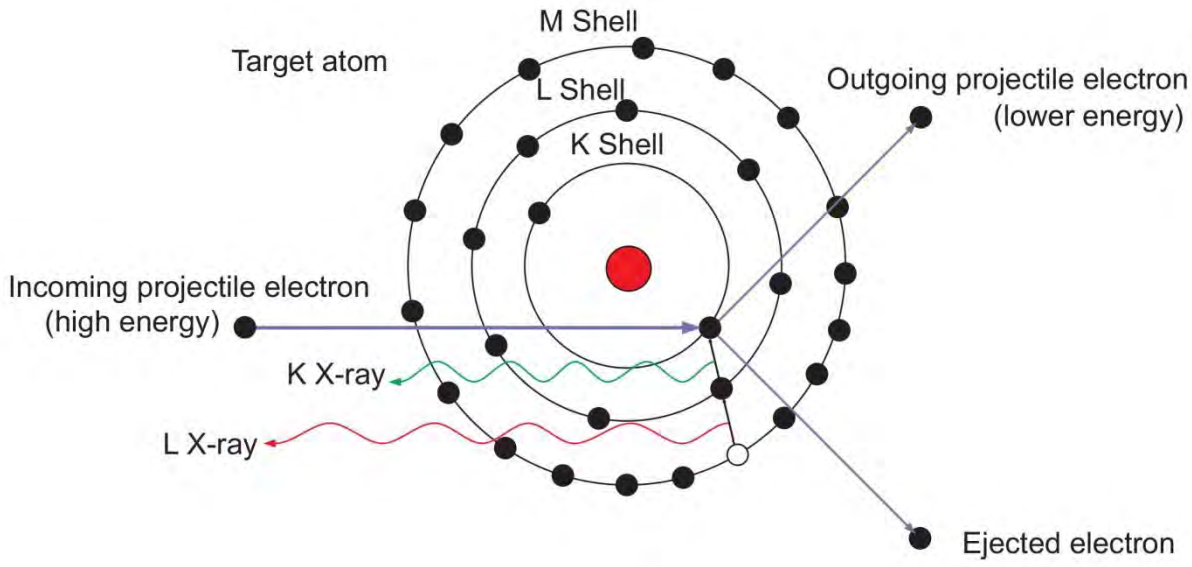

Figure 2. 3: Schematic diagram of characteristic X-ray production.

The efficiency of conversion is about 1 % or less of the total kinetic energy of the moving electrons (Chen et al., 2011). X-rays travel in a straight line and are not deflected by electric or magnetic fields. Exposure of photographic films to X-rays leads to darkening of the film and this phenomenon is applied in conventional screen-film imaging.

2.4 Evolution of CT scanners

CT scanners employed pencil-beam and few detectors in its primitive imaging ages. Now CT scanning has evolved from pencil-thin beam to the use of multiple detectors and slip ring technology for the acquisition of quality images (Kalender, 2005). This is portrayed in the various generational transformations from first generation scanning to spiral CT. Since the introduction of the fan beam, the major differentiating factors have been the detector width and gantry opening size. The modern clinical CT can acquire quality diagnostic images within a few seconds depending on the clinical examination task. A brief account of generational evolution of CT system provides an opportunity to re-examine how one might create ways of making the technique more effective, safe and beneficial to patients.

2.4.1 First Generation

Hounsfield, a computer engineer in England was the first to introduce CT scanners in the early 1970s (Kalender, 2005). A single highly collimated X-ray pencil-beam and detector is used to acquire data of X-ray transmissions (Cunningham et al., 2000). Each projection profile is obtained by translating the beam in a linear motion across the patient. After each projection, the detector and source are rotated one degree about the patient isocentre before another projection profile is taken. The scanning process is characterized by a translate-rotate motion of the source and detector through 180 degrees. Attenuated beam intensity after passing through the patient was evaluated by the detector from a sequence of

transmission measurements. An image was created from a total of 28,800 X-ray measurements acquired from 180 projections. The pencil beam geometry coupled with only two detectors was very efficient in reducing scatter radiation because scatter radiation was rejected by the other detector as shown in Figure 2.4. This advantage of first generation scanners was described as the best.

First generation CT detector configuration cannot be used in routine clinical scanning because of its long scan time (approximately 5 minutes) due to the complex scanning motion employed (Cunningham et al., 2000). Hounsfield used this geometry popularly known as parallel-beam geometry in his original experiment with gamma detectors (Hounsfield, 1973).

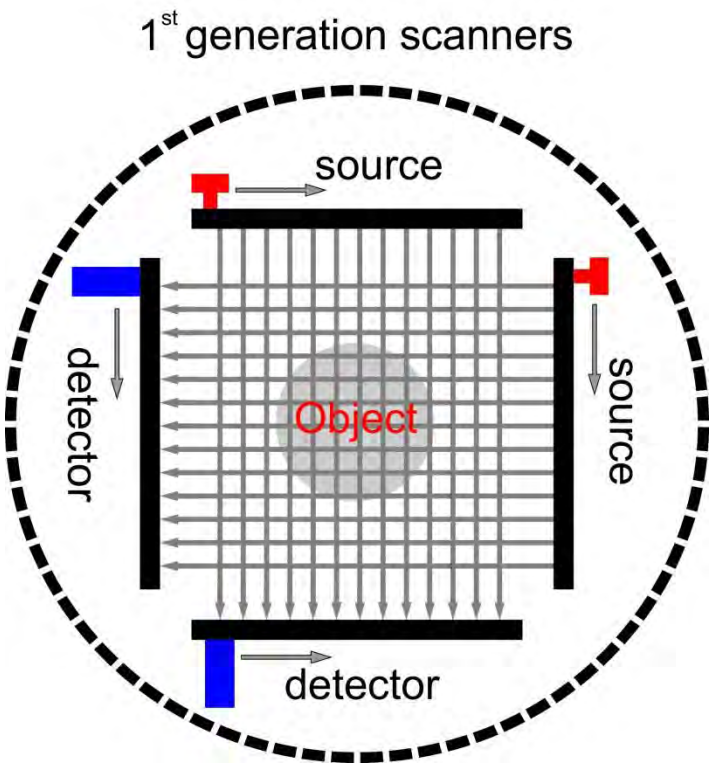

Figure 2. 4: Schematic diagram of the first-generation CT scanner

2.4.2 Second Generation

Second-generation CT scanners use a fan-beam of X-rays and a linear detector array to reduce the scan times by 30 seconds (Cunningham et al., 2000). Narrow fan-shaped beam geometry was used in place of the pencil beam together with multiple detectors. Even though a translate-rotate motion was used same as first generation, greater rotation per increment was used to achieve shorter scan times as shown in Figure 2.5. With improvement made, the second-generation CT scanners were not limited to only head scan protocols but a few body scans were also executed. Also, more complicated reconstruction algorithms were used to process fan-beam projection data. Even though the scan time was decreased, the amount of scatter radiation increased which is a disadvantage of the second-generation scanners.

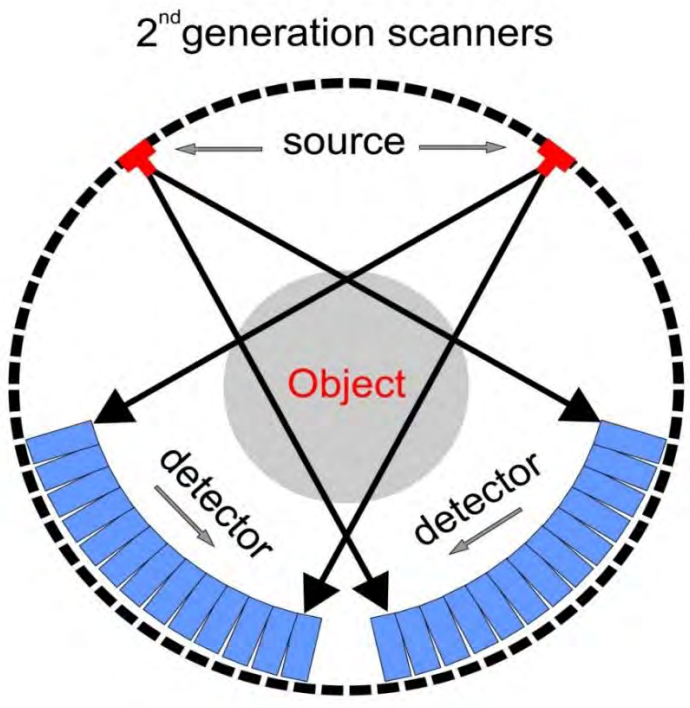

Figure 2. 5: Schematic diagram of the second-generation CT scanner

2.4.3 Third Generation

Introduced in the 1976, it has a fan-beam of X-rays that rotate 360 degrees around the isocentre (Cunningham et al., 2000). Uses a fan-beam wide enough to contain patient coupled with hundreds of independent detectors integrated into a curved detector array. The curved detector is mechanically coupled to the X-ray tube and both rotate together making it possible to obtain projection data for a single image in approximately 1 second as shown in Figure 2.6. 'Ring artefact' is a major problem associated with third generation CT scanners originating from the movement of detectors in the image acquisition process. Thin tungsten septa is usually placed between each detector and focused on the X-ray source to reject scattered radiation (Cunningham et al., 2000).

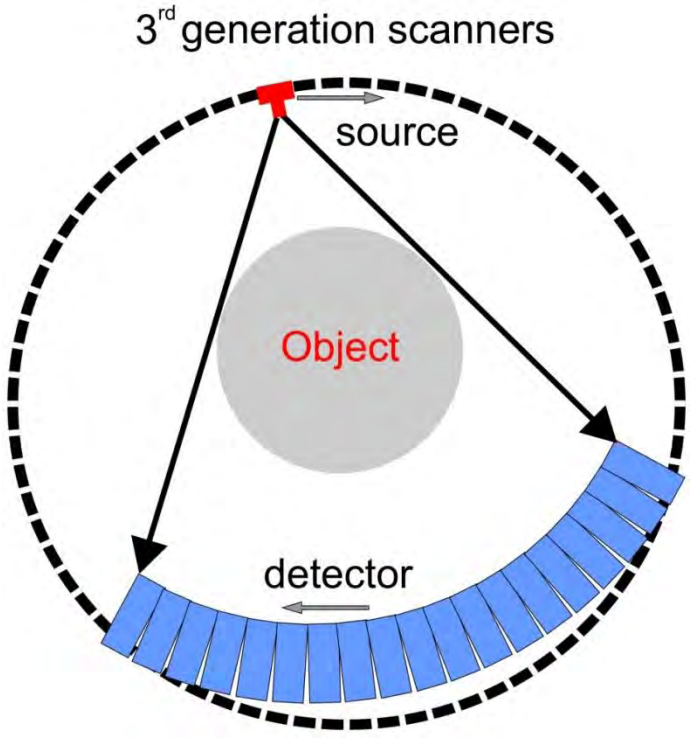

Figure 2. 6: Schematic diagram of the third-generation CT scanner

2.4.4 Fourth Generation

The configuration is such that, the detector array (600 to 4800 depending on the manufacturer) is stationary while the X-ray source and fan-beam rotate about the isocentre called rotate/stationary geometries (i) a rotating X-ray source outside a nutating detector array and (2) a rotating X-ray source inside a stationary detector array (Cunningham et al., 2000). Figure 2.7 shows the fourth generation scanner with the detector array forming a circle that surrounds the patient completely and has a scan time similar to that of third generation. Compared to third generation systems which has its detectors calibrated only once every few hours, fourth generation detectors are calibrated twice per X-ray tube rotation providing a self-calibrating system.

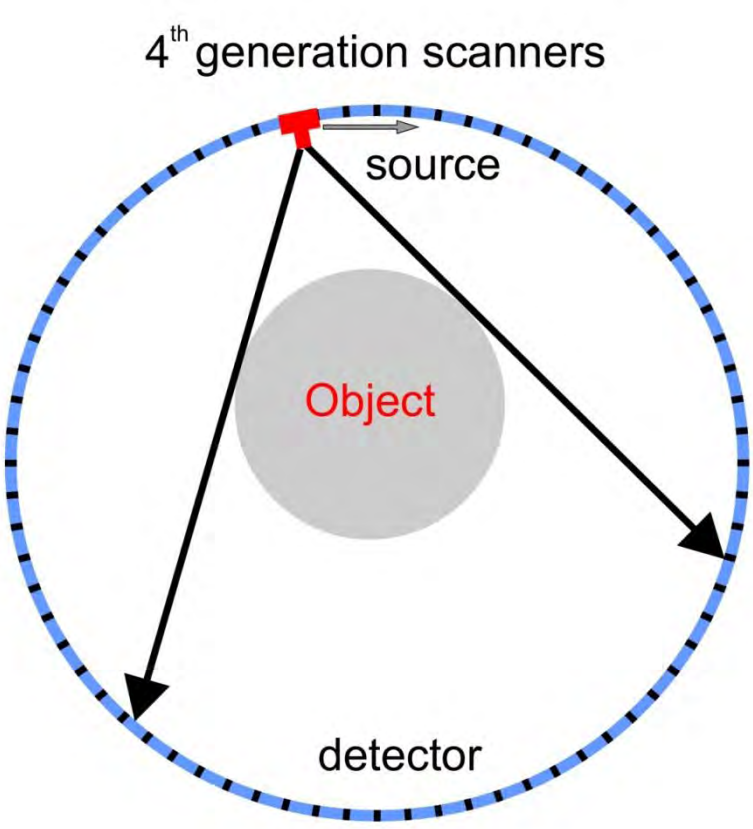

Figure 2. 7: Schematic diagram of the fourth-generation CT scanner

2.4.5 Fifth Generation

In fifth generation systems, the X-ray source is an integral part of the system design. In this geometry, the detector array remains fixed as a high-energy electron beam is electrically swept along a semi-circular tungsten strip anode thereby producing an X-ray source at the point where it hits the anode (Cunningham et al., 2000). The X-ray source is then rotated about the fixed patient as shown in the Figure 2.8. Fifth generation systems can be used to image a beating heart without significant motion artefacts because its projection data can be can be taken in approximately 50 ms. It is also called the Electron Beam Tomography (EBT) and can acquire about 17 images per second.

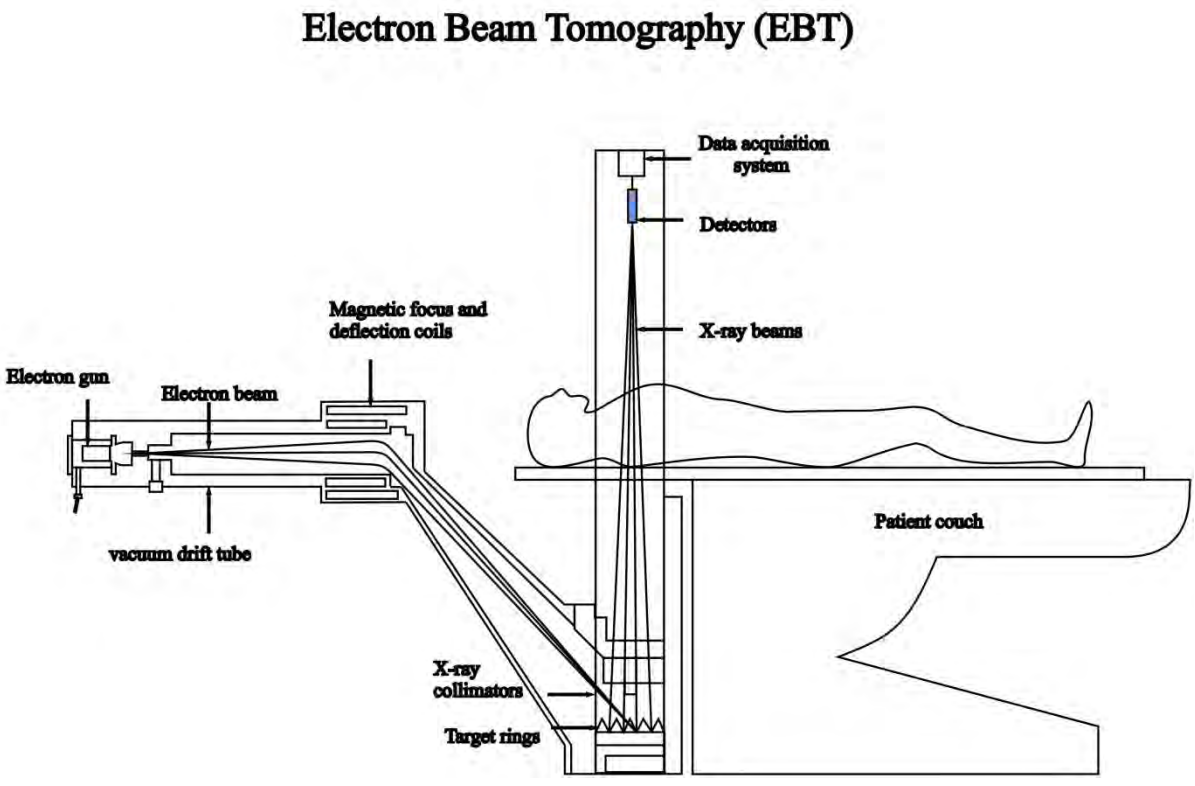

Figure 2. 8: Schematic diagram of the fifth-generation CT scanner

2.4.6 Sixth Generation/Helical CT

The advent of spiral scan has made it possible to have fast multiple scans in three-dimensional imaging. Self-lubricating slip-ring technology in third and fourth generation systems is used to make the electrical connections with the rotating components which allows for a continuous rotation of the X-ray fan-beam (Cunningham et al., 2000). Several images can therefore be acquired as the patient is transported smoothly through the gantry in a continuous motion as opposed to a step and shoot process. With this technology, the entire abdomen can be scanned within 30 seconds with reduced 'motion artefacts'. Here, data acquired is not in full slices because the scanner is not producing planar sections but can be compensated for in the reconstruction process. More sophisticated reconstruction algorithms are used here to accommodate the helical path outlined by the X-ray source as it goes round the patient.

2.4.7 Seventh Generation

Consists of multiple detector arrays and cone-shaped X-ray beam which does not pass through any narrow collimator. These generation of CT scanners are referred to as Multiple Computed Detector Arrays (MCDA), MDCT and MSCT. The intensity of the initial X-ray beam interacts more effectively with the multidetector array. The total scanning time is related to the total number of detectors which may range from 2 to 320 rows (Katada, 2002). The higher the number of detectors the lesser the total time of examination.

2.5 CT Dose Descriptors

Another advance of significance and which is a very common parameter used in CT dose estimation is the CTDI. It is commonly measured with pencil-shaped ionization chamber or other alternatives in cylindrical phantoms (Bauhs et al., 2008). It is important to understand the methods used in the estimation of radiation dose in this technology. It is expedient to measure dose in CT since users lack visual indication of overexposure as evident in screen-film radiographs. Dose descriptors are usually displayed by CT scanners and these include $CTDI_w$, Dose Length Product (DLP) and $CTDI_{vol}$. The introduction of CTDI (Shope et al., 1981) showed that with corrections for scan spacing, CTDI can be used to estimate Multiple Scan Average Dose (MSAD) which is the accumulated dose from multiple scan examinations. CTDI characterises the integral below the radiation dose profile from one axial scan, with the dose tails, divided by the nominal beam width NT, where N is the number of tomographic segments imaged at the same time per X-ray tube rotation, and T equals the width of each tomographic segment along the longitudinal z axis (Bauhs et al., 2008). CTDI is not does not represent dose at a point but rather an average dose for a given volume. This has made usage of CTDI for the measurement of dose from CT systems more popular. Mathematically, it is the integral along a line parallel to the axis of rotation (z) of the dose profile $(D(z))$ for a single slice given as:

$$CTDI = \frac{1}{T}\int_{-\infty}^{+\infty} D(z)dz \qquad (2.3)$$

Where T is the nominal reconstruction slice thickness (Hatziioannou et al., 2003). Pitch is defined as the ratio of table travel distance per rotation to the nominal beam width (ACR, 2008) and accounts for the table increment for each successive rotation. The unit of

measurement of CTDI is gray (Gy) and has submultiples including centigray (cGy) and milligray (mGy) respectively. The various forms of CTDI are described below.

2.5.1 $CTDI_{FDA}$

For MSAD to be theoretically equal to CTDI, all contributions from the tails of the radiation profile should be accounted for in the CTDI dose measurement. The U.S Food And Drugs Administration (FDA) first introduced $CTDI_{FDA}$ with the integration limits of ±7T, where T represents the nominal slice width. Even though the $CTDI_{FDA}$ could be used in dose measurement, it was limited to approximately fourteen slices (McCollough et al., 2009). Another dose index, the $CTDI_{100}$ was introduced as a solution to this problem. The $CTDI_{FDA}$ is calculated using the relation:

$$CTDI_{FDA} = \frac{1}{nT}\int_{-7}^{+7} D(z)dz \tag{2.4}$$

Where $D(z)$ is the dose allocation along the z-axis.

2.5.2 $CTDI_{100}$

The $CTDI_{FDA}$ had limitations which was overcome by the introduction of a calculated parameter of radiation dose, the $CTDI_{100}$. It represents a collection of a series of scan doses at the core of a 100 mm scan, which has the capacity of collecting doses for longer scan lengths. The $CTDI_{100}$ is larger than the $CTDI_{FDA}$ but smaller than the MSAD. The limits of

$CTDI_{100}$ start from -50 to +50 mm giving a range of 100 mm. The $CTDI_{100}$ equation is given below:

$$CTDI_{100} = \int_{-50}^{+50} \frac{D(z)}{N \times T} dz \tag{2.5}$$

Where $D(z)$ is the dose allocation along the z-axis, T is the slice width and N is the number of slices imaged for each axial scan.

2.5.3 $CTDI_w$

Distribution of dose over the cross section of the body in a CT scan is much more homogeneous than that of radiography. The dose is however evenly distributed across the surface and decreases towards the centre. Weighted CTDI ($CTDI_w$) is a subjective standard of the $CTDI_{100}$ at the centre and the periphery of a standard Polymethyl Methacrylate (PMMA) phantom used to estimate patient dose.

Calculations for the weighted $CTDI_w$ normalizes it to 100 mAs and does not account for effects of pitch or gaps in helical CT scan given as:

$$CTDI_W = \frac{1}{3}(CTDI_{100,center} + \frac{2}{3} CTDI_{100,edge}) \tag{2.6}$$

2.5.4 Multiple Scan Average Doses (MSAD)

MSAD represents the average dose over one scan interval (I) at the centre of a multiple scan (N) dose profile where the initial and final scans contribute insignificant dose to the

central region (Bauhs et al., 2008). The MSAD basically describe the CT dose and the sequence of CT scans achieved on a patient. MSAD can be calculated using the equation given below:

$$MSAD = \frac{N \times T}{I} \times CTDI \tag{2.7}$$

Where, N represents the number of scans, T is the slice width (mm) and I is the interval between scans (mm).

For MSCT system $N\ x\ T$ is the total beam width and I represents the patient table feed during one gantry rotation. Thus, for spiral scan, the MSAD is given as:

$$MSAD = \frac{1}{pitch} \times CTDI \tag{2.8}$$

Theoretically, MSAD and CTDI are equivalent if the pitch is equal to unity. The value of MSAD can be averaged over a single scan interval at the centre of the profile. Figure 2.9 shows radiation dose profiles consisting of nine axial CT scans which are adjacent to each other along a line perpendicular to the axial scans.

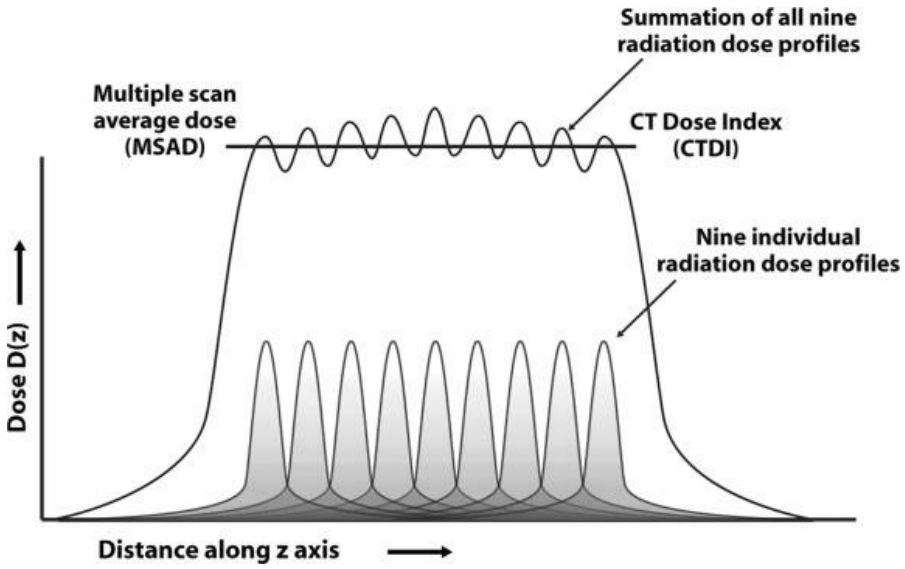

Figure 2. 9: The radiation dose profiles (Bauhs et al., 2008).

2.5.5 Volume CT dose index ($CTDI_{vol}$)

Scanner output of a specific scan protocol is estimated by $CTDI_{vol}$ given as:

$$CTDI_{vol} = \frac{1}{p} CTDI_W = \frac{1}{3p} (CTDI_{100,center} + 2CTDI_{100,edge}) \quad (2.9)$$

To account for travel distance per gantry rotation and nominal beam width it is written as:

$$CTDI_{vol} = \frac{nT}{I} CTDI_W = \frac{1}{p} CTDI_W \quad (2.10)$$

Where n is the number of section for each scan and w is the nominal beam width (Bauhs et al., 2008).

2.5.6 Dose-Length Product (DLP)

It is a better representation of the overall energy delivered by a given scan protocol by the integration of the $CTDI_{vol}$ along the scan length. Where the DLP (in mGy-cm) is equal to the product of $CTDI_{vol}$ (in mGy) and scan length (in cm) given below:

$$DLP = CTDI_{vol} \times Scan\,length \tag{2.11}$$

The DLP reflects the integrated radiation output attributable to the complete scan protocols. The DLP differs from one scanner type to another and the image quality desired. Also, a change in technique (such as varying pitch, kVp or mA) also changes the value of DLP.

2.5.7 Estimation of Organ and Effective Dose (ED)

In the 1990's the effective dose, as defined in ICRP 60 and later redefined, became a useful tool for comparing absorbed-dose levels between X-ray radiography and CT or different CT scan protocols(ICRU, 2012). ED is not a physical dose metric but used to describe the level of organ radio-sensitivities. The fact that effective dose includes weighting factors that are derived from radiobiological considerations in its computation does not make it a physical dose. ED was therefore not proposed for the assessment of an individual patient's radiation dose, since the radiobiological weighting factors are not related to a specific patient. It is a concept used to normalize partial body irradiations comparative to whole body irradiations to allow assessments of risk. The calculation of ED involves knowledge of doses to organs at risk within the body, and can be obtained from "Monte Carlo modelling" of absorbed organ doses inside mathematical anthropomorphic phantoms as

well as voxel phantoms created from real humans. Effective dose is stated in millisieverts (mSv) and is comparable to effective dose from various sources of ionizing radiation. An example is background radiation level, which is typically in the range of one to three mSv depending upon the location.

Effective dose is given by the equation:

$$ED = K \times DLP \tag{2.12}$$

Where, ED is the effective dose in mSv, and K is the conversion factor measured in, mSv x (mGy^{-1} x cm^{-1}) dependent on the body region imaged.

The radiation protection quantity equivalent dose in an organ or tissue, H_T, is then defined by:

$$H_T = \sum_R W_R D_{T,R} \tag{2.13}$$

where W_R is the radiation weighting factor for radiation R shown in Table 2.1.

Organ dose can be obtained using the effective dose from the equation:

$$E = \sum_T W_T \sum_R W_R D_{T,R} = \sum_T W_T H_T \tag{2.14}$$

Where;

W_R is the radiation weighting factor

W_T is the tissue weighting factor

Table 2. 1: Tissue weighting factors, W_T, in the 2007 recommendations.

Tissue	Tissue weighting factor, W_T
Gonads	0.08
Bone marrow	0.12
Colon	0.12
Lungs	0.12
Stomach	0.12
Bladder	0.04
Breast	0.12
Liver	0.04
Oesophagus	0.04
Thyroid	0.04
Skin	0.01
Bone surface	0.01
Brain	0.01
Salivary glands (brain)	0.01
Remainder	0.12
Total	1

Table 2. 2: Radiation weighting factors in the 2007 recommendations

Radiation type	Radiation weighting factor w_R
Photons	1
Electrons and muons	1
Protons and charged pions	2
Alpha particles, fission fragments, heavy ions	20
Neutrons	A continuous curve as a function of neutron energy

Table 2. 3: Shows normalised effective dose per dose-length product (DLP) for adults (standard physique) and paediatric patients of different body regions according to the AAPM Report 96.

Region of body	k (mSv mGy^{-1} cm^{-1})				
	0-year-old	1 year old	5-year-old	10-year-old	Adult
Head and neck	0.013	0.0085	0.0057	0.0042	0.0031
Head	0.011	0.0067	0.004	0.0032	0.0021
Neck	0.017	0.012	0.011	0.0079	0.0059
Chest	0.039	0.026	0.018	0.013	0.014
Abdomen & pelvis	0.049	0.03	0.02	0.015	0.015
Trunk	0.044	0.028	0.019	0.014	0.015

2.5.8 CT Protocol

Past research also indicates that CT scan parameters can be altered to optimize dose to patients including tube current, tube potential, detector configuration, pitch, reconstruction algorithm, patient positioning, scan range and reconstructed slice thickness (Chen et al., 2017). A good manipulation of these parameters may have the advantage of safer imaging of patients in terms of dose delivered per examination procedure without appreciable loss of diagnostic image quality. Tube current basically regulates the amount of electrons striking the anode thereby affecting the number of X-rays emitted (Zink, 1997). The flow of electrons between the cathode and anode components of the X-ray tube constitutes the tube current. Radiation dose delivered to patients is directly proportional to the mA used in the scanning process. Meanwhile the magnitude of the mA does not show in the image as seen in conventional X-ray imaging in the degree of brightness or darkness of the image. The operators' failure to choose the appropriate mA settings will consequently lead to high

radiation dose being delivered to the patient. Similar to other imaging modalities, there are technique charts that the operator must refer to that serve as a guide to selection of appropriate acquisition parameters for a particular scanning procedure. All the acquisition parameters in CT can be altered to deliver the right amount of dose and obtain the required diagnostic image quality. In view of this, operators usually standardize the kVp and gantry rotation time (s) while selecting the mA as a function of the patient size since it is the key parameter that is adapted to patient size. McCollough et al. (2006) have shown that the mA should be adjusted to correlate to the total attenuation of the anatomy of interest but not the patient weight. An exception of the anatomical structures is the head in which attenuation is relatively distinct due to age owing to the fact that attenuation basically comes from the nature of the bones of the skull which is age dependant (Galanski et al., 2005). Acquisition techniques play significant roles in dose reduction and image quality and are worth discussing.

2.5.8.1 Tube Current

FTC for example, is a technique particularly of interest to this study. It does not account for tremendously large variations that occur in patient absorption regarding anatomic region and projection angle. Considering the fact that noise in the final image is basically determined by the projection with the most noise, substantially less radiation can be used in data acquisition through body parts having less attenuation or projections of limited interest without negatively affecting the final image noise. Tube current is modulated to adapt to the attenuation variations within the patient which may occur along the axis of the patient, angularly about the patient or a combination of both.

Automatic Exposure Control (AEC) as an aspect of tube current modulation is an automatic adaptation of the mA to attenuation differences within the patient based on user-defined adjustments for different spatial projections or at specified times (Keat, 2005). It is expedient to separate paediatric and adult protocols when switching to AEC from fixed mA. This is because children are more prone to radiation induced adverse effects than for adults hence lower dose settings of AEC required. Advanced MDCT scanners employ three kinds of spatial mA modulations; angular (x, y) mA modulation, longitudinal (z) mA modulation and a combined angular and longitudinal (x, y, z) mA modulation (Keat, 2005).

Angular modulation also known as x-y or transverse modulation is also a technique that adjusts mA at different projections within each gantry rotation. This technique determines cross-sectional attenuation characteristics of the scanned body region from either the localizer radiographs or the preliminary one-half gantry rotation of the X-ray tube (Keat, 2005). The technique decreases mA in other projections accompanied with lower X-ray attenuation as compared to attenuation of X-rays from the projections with the greatest attenuation. In chest CT, the greatest attenuation at the shoulder level occurs in the lateral projections, allowing the technique to maintain constant noise while reducing mA at other projections. In general, x-y modulation is applied by specifying mA just as for fixed-mA examinations and switching on the x-y modulation feature on the scanner user interface. Longitudinal or z-axis modulation applies localizer radiographs to determine attenuation properties of the scanned body at varying locations along the patient length (Keat, 2005). The mA is modulated (increased or decreased) at z-axis positions based on user-specified image quality metric and attenuation characteristics of specific body regions. Combined (Angular and longitudinal) mA modulation is also of significance. The x-y-z

modulation technique is a combination of the x-y and z modulation techniques used to adjust mA values in all 3 axes based on user specified image quality and attenuation characteristics of the various locations of the body being scanned (Keat, 2005). The x-y-z modulation technique has the advantage of greater dose reduction accounting for both cross-sectional asymmetry and longitudinal variations in attenuation along the scanned body region. As applicable to the x-y or z modulation, users must specify an image quality metric when using x-y-z modulation technique. As regards the various modes of operation of different AEC systems CT manufacturers have developed their own techniques and application capabilities on their systems (Söderberg and Gunnarsson, 2010). The objective is to reduce radiation dose thereby protecting the patient from undue radiation exposure while maintaining diagnostic image quality, elimination of photon starvation artefacts and reduced load on the X-ray tube (Kulama, 2004). One of the popularly used systems that was applied in the study is discussed below.

CARE Dose 4D is a combined tube current modulation system used on Siemens (Söderberg & Gunnarsson, 2010). Based on the patient's size and shape the system automatically modulates the tube current with real time, online, controlled tube current modulation during each rotation. Anterior-posterior or lateral attenuation profile (anatomic shape, size and attenuation at each location) along the patient's long axis (z-axis) is measured based on a single CT localizer radiograph, "tomogram", in the direction of the projection and calculated for the vertical direction using a mathematical algorithm (Söderberg and Gunnarsson, 2010). The CARE Dose 4D has sufficient image noise according to Siemens modulation, which varies base on the patient's size and shape. The operator has the option of choosing any level of tube current, selected according to the

patient's size, using 'weak', 'average' or 'strong' settings to control the amount of mA supplied and this defines the image quality. The manufacturer sets the default adaptation strengths to average decrease for slim and average increase for obese sections. The CARE Dose 4D modulations are capable of providing a lower tube current to keep image noise consistent regardless of the patient size or anatomical variations (Keat, 2005).

2.5.8.2 Tube Potential

Tube potential is the difference in electrical potential between the anode and cathode of the X-ray tube. It is normally known as peak kilovoltage or kVp and measured in voltage. The energy of photons coming from the anode is determined by the energy of electrons striking the anode which is regulated largely by the peak voltage. Image contrast can be increased by reducing the tube potential especially for iodine-enhanced CT examinations. This is due to the dependence of image contrast on the effective atomic number (Z) of the scanned material or tissue. For example, iodine with a higher Z of 53 has its image contrast affected more at lower tube potential than water with a lower effective Z of 7.4. This effect is attributable to photoelectric interactions that result in difference in linear attenuation coefficients for materials with different atomic numbers. The magnitude of photoelectric interactions is related directly to the cube of the atomic number (Z) and inversely related to the cube of the photon energy. Lower tube potential can be used for patient size below some threshold to obtain same image quality as high tube potential image quality with the advantage of lower radiation dose. However, a reduction in tube potential leads to increase in image noise but unlike tube current, the noise can be mitigated to some level by improved image contrast. The lung tissue is less sensitive to image noise and has higher

contrast affording the possibility of being scanned at lower tube potential compared with other anatomical structures such as head and abdomen. For instance performing pulmonary CT angiography (CTA) at lower tube potential (80-100 kV) enhances contrast in the pulmonary vasculature (Hennequin et al., 2004; Szucs-farkas et al., 2008). Szucs-Farkas et al. (2008) stated higher attenuation values in the pulmonary arteries when scanned at 80 kV compared with 100 kV. Tube potential can therefore be optimized for small adults and children as well as CTA.

2.6 Paediatric Computed Tomography

The discussions so far clearly demonstrates that CT usage has definitely accelerated over the last half century and has introduced a lot of technological advancements since the introduction of this technology and has improved speed and image acquisition (Hatziioannou et al., 2003). This has enhanced the evaluation of younger and difficult children as well as reduced the need for sedation in paediatrics CT examinations (Hatziioannou et al., 2003). It is crucial to evaluate radiation dose to children most importantly because children are relatively more radiosensitive to ionizing radiation because of higher sensitivity to cell damage due to cell division being more active in children. Also some radio-sensitive organs such as the bone marrow represent a greater percentage of the total body mass of children making them more vulnerable to radiation-induced cancer (Ledenius, 2011). Notwithstanding the great benefit gained from the diagnostic information obtained from CT examinations, the radiation dose delivered to paediatrics cannot be disregarded because the radiobiological implications are significant

(Boone et al., 2011). Due to long life expectancy in children there is a greater tendency of biological effects of radiation manifesting in children.

A study made in Africa in 2009 estimated that paediatric CT accounted for about 20% of all CT examinations (Muhogora et al., 2009). It is obvious these statistics will shoot up in the near future and therefore have to be addressed accordingly. Also a study that assessed the lifetime cancer mortality risks due to radiation from CT showed a higher risk to paediatric (Brenner et al., 2001). Paterson et al. (2001) tried to determine whether patient age was considered in selecting the scanning parameters that are determinants of radiation dose for helical CT of paediatric patients and reported that paediatric CT parameters were not adjusted based on age or examination type indicating that children may be exposed to unnecessarily high radiation during CT scan. This view was supported by Galanski et al. (2005) who suggested that for paediatric head CT, adjustments be made based on age since the size of the head is overly large in infants and children. Notwithstanding the fact that children are more sensitive to ionizing radiation, they are at greater risks of receiving higher organ doses compared to adults since their bodies attenuate lesser photons before reaching the organs of interest, resulting in higher energy deposition per unit mass (Ledenius, 2011).

Developments and advances in techniques and procedures discussed in this chapter may suggest that CT scan has come far enough as an effective means of providing a safe imaging tool in the medical field. While there is some truth in this assertion, it is also clear that the level of safe delivery could be much more improved than it is at the moment. The challenge of the study is to suggest alternative ways to refine some of the current level of delivery by examining selected results, their implications and possible ways of radiation dose reduction

and acquisition of substantially improved image quality. The method of approach to the challenge is the subject of the next chapter.

CHAPTER THREE

3.0 MATERIALS, METHOD AND PROCEDURES

Overview

This chapter describes the materials used and methods used to carry out the study focussing on adult and paediatric chest examinations performed with PMMA head and body phantoms using a 16 slice Siemens CT scanner at 110 kVp applying AEC and FTC techniques.

3.1 Materials

Each of the equipment and resource materials used and their relevance to the study are listed, described and discussed below.

1. 16 slice Siemens CT scanner (Siemens Somatom Emotion, Forchhiem, Germany).
2. CT dose profiler probe (RTI Electronics, Sweden).
3. Standard CT dosimetry PMMA cylindrical acrylic head and body phantom (PTW, Freighburg, Germany)
4. Microsoft Excel (2016) and SPSS version 25.0 (2017).
5. CT-Expo v2.5 software.
6. The Sweden Ghana Medical Centre supported the study with available resources.

3.1.1 The CT scanner

A 16 slice Siemens CT scanner (Siemens Somatom Emotion, Forchhiem, Germany) was used for the examinations by simply selecting a predefined scan protocol (Figure 3.1). In this experiment spiral scanning was employed at 110 kVp with AEC and FTC techniques. It has a16 channel detector configuration with a very small focal spot (0.8 x 0.5 mm) capable of 16 x1.2 mm multi-slice imaging.

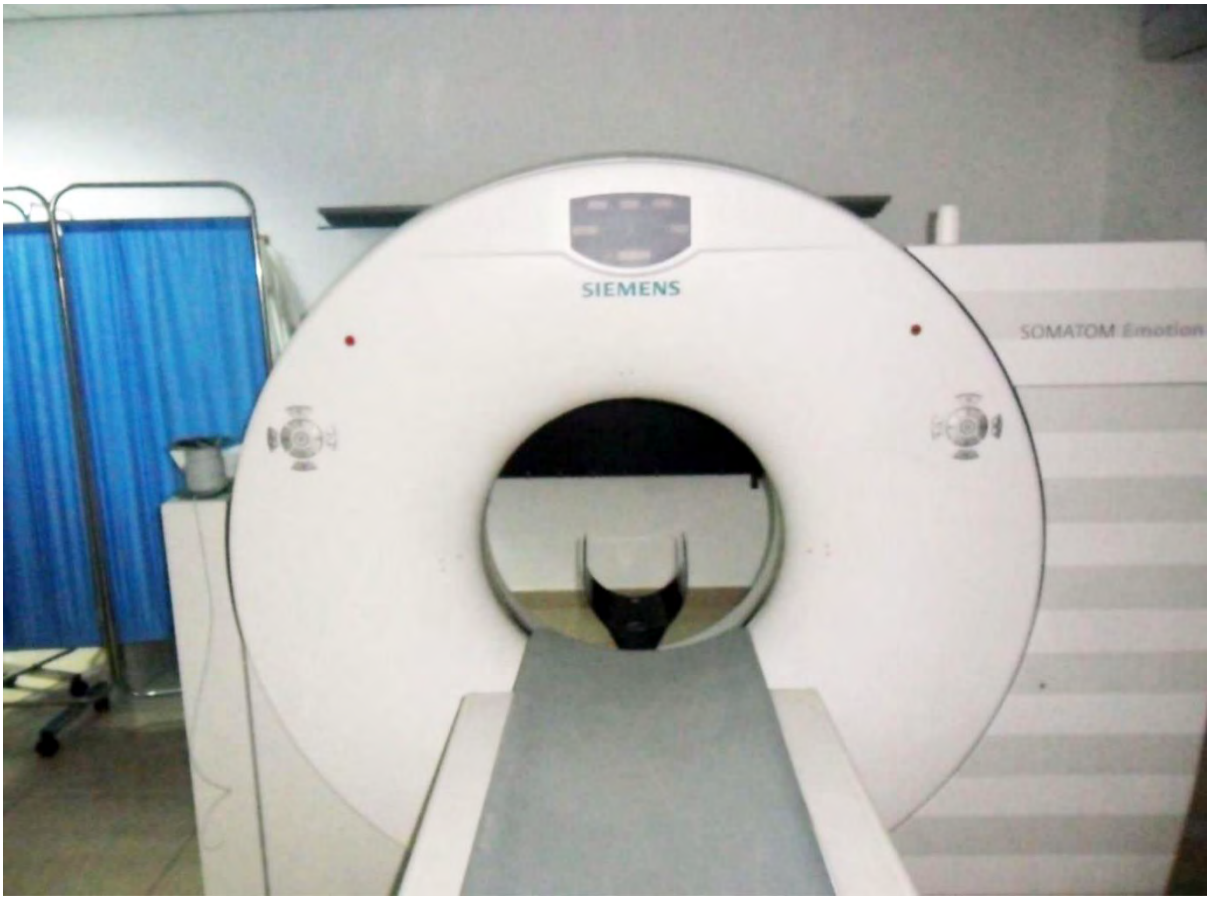

Figure 3. 1: Picture of a 16 slice Siemens Somatom Emotion CT scanner [Field work, 2018].

3.1.2 CT Dose Profiler Probe (CTDP)

The CT dose profiler probe is a detector device used to measure point doses and has a solid-state sensor located 3 cm from the end of the probe. It was connected to the barracuda for dose measurements by the Ocean software using dose values registered by the detectors of the sensor as radiation hits it. The technical specifications of the CTDP are given in Table 3.1 below.

Table 3. 1: Specifications of the CTDP.

Supported meters:	Barracuda with EMM-1Ch, EMM-2Ch, EMM-Bias, EMMBiasB and EMM-BiasW (with Ocean) Piranha with external input (with Ocean 2014)
Typical cal. factor:	0.28 mGy/nC
Material:	Al and PMMA
Connector:	Triaxial LEMO
Length (Detector + extension):	165 mm + 45 mm
Diameter:	12.5 mm
Sensor width:	250 um
Max sensitivity variation:	Less than ±5 %
Weight (Probe + extension):	40 g + 10 g

3.1.3 PMMA Dosimetry Phantoms

CTDI measurements were made using head and body PMMA dosimetry phantoms. The 16-cm diameter head phantom was used for the children acquisitions and the 32-cm diameter body phantom represented the adult body. The CTDP was placed in the 1-cm holes located at the centre for dose measurements shown in Figure 3.2.

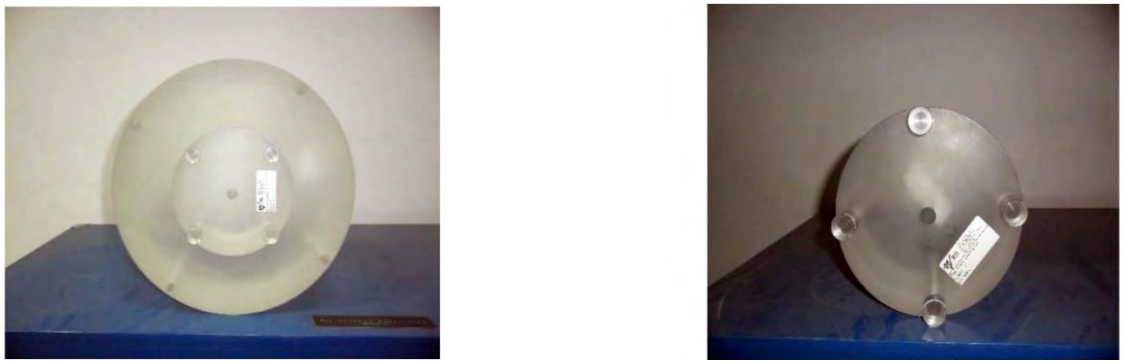

Figure 3. 2: Picture of body phantom (left) and head phantom (right) [Field work, 2018].

3.2 Experimental Method

3.2.1 CT Protocol

Dose measurements were performed for routine chest CT examination protocols with AEC and FTC techniques. The routine scan protocols used for the CT examinations are presented in Tables 3.2, 3.3 & 3.4.

Table 3. 2: Protocol for AEC technique for routine body examinations.

Protocol	Head	Thorax	Abdomen	Pelvis	Spine
kVp	110	110	110	110	110
Effective mAs	25	25	25	120	120
Rotation Time (s)	0.6	0.6	0.6	0.6	0.6
Slice Thickness (mm)	3	3	3	3	3
Pitch Factor	0.55	0.8	0.8	0.8	0.8
Reconstruction Slice	1.5	1.5	1.5	1.5	1.5
Kernel	T20s	T20s	T20s	T20s	T80s
Acquisition	16.0 x 0.6	16.0 x 0.6	16.0 x 0.6	16.0 x 0.6	16.0 x 0.6

Table 3. 3: Protocol used for adult chest CT examination using FTC technique.

Examination	kVp	mAs	Rotation Time (s)	Pitch Factor	Slice Thickness (mm)
Body	110	65	0.6	0.8	3
Body	110	75	0.6	0.8	3
Body	110	86	0.6	0.8	3
Body	110	95	0.6	0.8	3
Body	110	105	0.6	0.8	3

Table 3. 4: Protocol used for paediatric chest CT examination using FTC technique.

Examination	kVp	mAs	Rotation Time (s)	Pitch Factor	Slice Thickness (mm)
Body	110	16	0.6	0.8	3
Body	110	21	0.6	0.8	3
Body	110	26	0.6	0.8	3
Body	110	31	0.6	0.8	3
Body	110	36	0.6	0.8	3

3.2.2 Measurement of Dose with the CTDP

The adult body phantom was first set up on the CT couch and focused at the isocentre of the scanner with the help of the z-axis of the scanner by aligning the long axis of the phantom with it. The CTDP was connected to a barracuda with a cable and inserted into the central hole of the dosimetry body phantom with the extension end forward. The sensor of the CTDP was aligned with the central line on the phantom. A tape was placed on the

surface of the phantom at the terminal end of the central hole to prevent the probe from moving to any exposure. The barracuda was connected to a computer with a modern ocean software. The phantom together with the inserted CTDP set-up was aligned on the couch with the help of the two horizontal lasers in the CT room by adjusting them such that they appear on the mid-line of the CTDP as shown in Figure 3.3. The vertical lines were also set at the middle of the phantom. Precaution was taken to prevent removal of the CTDP from the phantom by using tapes to hold the cables that connect the CTDP and the phantom to the couch. Also, the CT room was closed to prevent background radiation from interference.

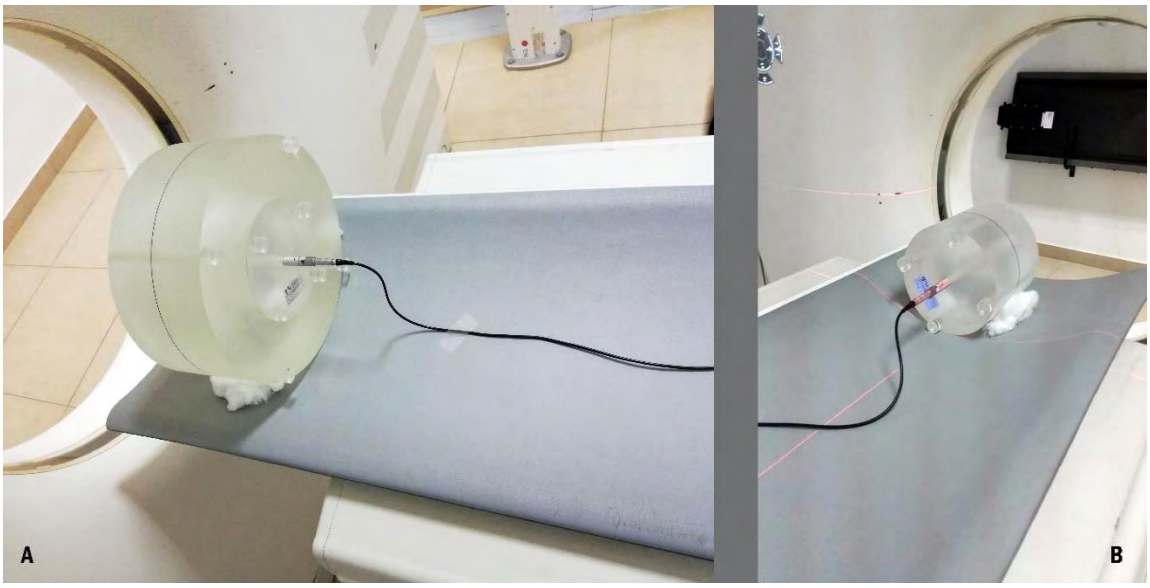

Figure 3. 3: Experimental Setup for measurement of dose. A. Adult body (32 cm diameter). B. Paediatric body (16 cm diameter) [Field work, 2018].

Standard routine patient protocol for chest examinations was selected for the measurements. A scout of the phantom was performed and the area about the phantom where measurements was to be taken was marked serving as the field of view

(FOV)(Figure 3.4). The mark began just before the phantom and ended just after the phantom. The barracuda was put on and then connected at the ocean software interface. The CT manufacturer and type was selected on the software interface to obtain the right k-factor. The measuring parameters were set on CT and the same was entered into ocean. Measurement for both CT and ocean was started at the same time taking into consideration the delay on CT.

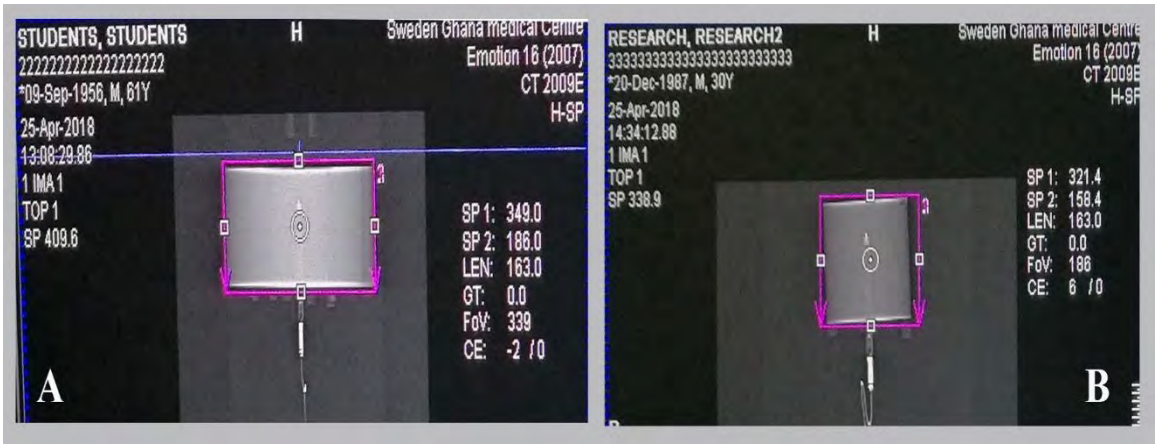

Figure 3. 4: A scout of the phantoms used for selection of FOV. A. Adult body (32 cm diameter). B. Paediatric body (16 cm diameter) [Field work, 2018].

The first scan was done with the standard protocols of routine body CT examinations with AEC activated as shown in Table 3.2. The body scan for adult phantom was repeated with manual selection of effective current (65 mAs, 75 mAs, 86 mAs, 95 mAs, 105 mAs) keeping all other parameters constant (Table 3.3). Similar scan procedure was repeated for the paediatric body (16 cm diameter head phantom) with manual selection of effective current (16 mAs, 21 mAs, 26 mAs, 31 mAs, 36 mAs) keeping all other parameters constant (Table 3.4).

The range of data points chosen was above and below the default setting in order to evaluate its influence on dose as well as check the functionality of AEC system. Weighted CT dose index ($CTDI_w$), Dose length product (DLP) and volume-weighted CT dose index ($CTDI_{vol}$) values obtained during each scan of the adult and paediatric chest examinations were recorded. The data obtained was saved as real time displays.

3.3 Organ and Effective Dose Estimation

The CT-Expo software V2.5 (Stamm & Nagel, 2017) was used to calculate the radiation dose of the mathematical phantom shown in Figure 3.5. The CT-Expo V 2.5 is an MS Excel application programmed in Visual Basic for the calculation of patient dose in CT examinations. Dosimetry data obtained from scans of the head and body phantoms were inputted into the CT- Expo software. The input data included CT scan manufacturer, model, patient age group, patient sex, selection mode. Scanning parameters included; kVp, mAs, reconstructed slice thickness, number of scan series, total collimation, table feed and scan length. ED calculation was based on the organ dose conversion factors of ICRP 103.

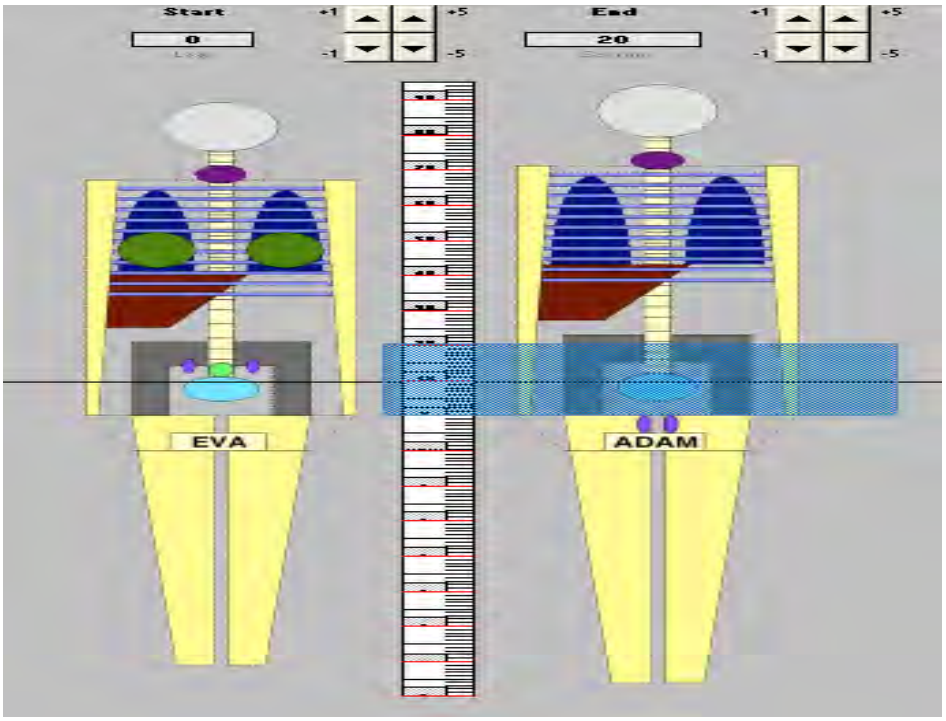

Figure 3. 5: The phantom models used in the CT-Expo for calculation of the organ and ED in the chest scans (Stamm and Nagel, 2017).

3.4 Determination of Dose Reduction (DR)

$CTDI_{vol}$ and DLP values were recorded as radiation dose delivered for both AEC and FTC techniques. Radiation dose reduction was estimated from the $CTDI_{vol}$ and DLP values by calculating the difference between these values for AEC and FTC techniques in percentage as shown in the equations below. $CTDI_{vol}$ relation is given as:

$$DR = \frac{CTDI_{vol\,Fix\,mA} - CTDI_{vol\,AEC}}{CTDI_{vol\,Fix\,mA}} \times 100\% \qquad (3.1)$$

Where;

$CTDI_{vol\,Fix\,mA}$ is the $CTDI_{vol}$ value for a particular fixed effective tube current value.

$CTDI_{vol\,AEC}$ is the $CTDI_{vol}$ value for the AEC effective tube current value.

DLP relation is given as:

$$DR = \frac{DLP_{Fix\,mA} - DLP_{AEC}}{DLP_{Fix\,mA}} \times 100\% \qquad (3.2)$$

Where;

$DLP_{Fix\,mA}$ is the DLP value for a particular fixed effective tube current value.

DLP_{AEC} is the DLP value for the AEC effective tube current value.

3.5 Data Analysis

Microsoft Excel (2016) and SPSS version 25.0 (2017) was used for statistical analysis of the data collected as well as the results obtained. SPSS was used to create clustered boxplot of organ doses to compare doses resulting from the two techniques employed (AEC vs FTC). Microsoft Excel spreadsheet was used to perform paired t-test to compare the DLP and $CTDI_{vol}$ between the AEC and FTC techniques.

CHAPTER FOUR

4.0 RESULTS AND DISCUSSION

This chapter presents the results obtained and the relevant discussions based upon the literature review.

RESULTS

4.1.1 Measured CTDI values using CTDP

The results of $CTDI_{vol}$ and DLP values obtained from an average of three measurements in the PMMA dosimetry phantoms scan using the CTDP with AEC and FTC techniques for adult and paediatric chest CT examinations are presented in Tables 4.1 and 4.2 respectively.

Table 4. 1: Dose measurements for adult chest CT examination with AEC and FTC techniques at 110 kVp.

Scanning type	**$CTDI_{vol}$ (mGy)**	**DLP (mGy-cm)**
AEC	6.77	110.40
65.00	5.11	83.35
75.00	5.89	95.97
95.00	7.48	121.90
105.00	8.28	135.00

Table 4. 2: Dose measurements for paediatric chest CT examination with AEC and FTC techniques at 110 kVp.

Scanning type	$CTDI_{vol}$ (mGy)	DLP (mGy-cm)
AEC	2.58	42.04
26.00	3.52	57.25
31.00	4.31	70.20
36.00	5.12	83.50

4.1.2 Console Displayed CTDI values

The results of $CTDI_{vol}$ and DLP values displayed at the CT console during measurements in the PMMA dosimetry phantoms scan with AEC and FTC techniques for adult and paediatric chest CT examinations are presented in Tables 4.3 and 4.4 respectively.

Table 4. 3: CTDI and DLP values displayed at the console for adult chest CT examination with AEC and FTC techniques at 110 kVp.

Scanning type	$CTDI_{vol}$ (mGy)	DLP (mGy-cm)
AEC	6.94	124.26
65.00	5.21	93.20
75.00	5.98	107.12
95.00	7.60	136.04
105.00	8.38	149.97

Table 4. 4: CTDI and DLP values displayed at the console for paediatric chest CT examination with AEC and FTC techniques at 110 kVp.

Scanning type	$CTDI_{vol}$ (mGy)	DLP (mGy-cm)
AEC	1.68	29.99
16.00	1.32	23.57
26.00	2.09	37.49
31.00	2.51	44.99
36.00	2.87	51.42

4.1.3 CTDI values simulation with CT-Expo

The results of $CTDI_{vol}$ and DLP values obtained from CT-Expo simulations with AEC and FTC techniques for adult and paediatric chest CT examinations are presented in Tables 4.5 and 4.6 respectively.

Table 4. 5: CTDI and DLP values obtained from the CT-Expo simulations for adult chest CT examination with AEC and FTC technique at 110 kVp.

Scanning type	$CTDI_{vol}$ (mGy)	DLP (mGy-cm)
AEC	5.3	166
65.00	4	125
75.00	4.6	144
95.00	5.8	183
105.00	6.4	202

Table 4. 6: CTDI and DLP values obtained from the CT-Expo simulations for paediatric chest CT examination with AEC and FTC technique at 110 kVp.

Scanning type	**$CTDI_{vol}$ (mGy)**	**DLP (mGy-cm)**
AEC	2.7	58
16.00	2.1	44
26.00	3.3	72
31.00	4	86
36.00	4.6	100

4.1.4 Comparison of CTDI values

The results of $CTDI_{vol}$ and DLP measurements for adult chest examinations obtained from the CTDP and that from CT-Expo simulations were compared to the displayed values at the CT console as presented in Table 4.7. From the percent deviations calculated, $CTDI_{vol}$ and DLP values from the CTDP deviated by 1.71 and 10.50 % and that from CT Expo simulations deviated by 23.40 and -34.44 % respectively from the CT console displayed values.

Table 4. 7: Deviation of measured and simulated $CTDI_{vol}$ and DLP values for adult chest CT examination at 110kVp.

Scanning Type	Console Displayed $CTDI_{vol}$ (mGy)	Console Displayed DLP (mGy-cm)	CTDP $CTDI_{vol}$ (mGy)	CT Expo $CTDI_{vol}$ (mGy)	CTDP DLP (mGy-cm)	CT Expo DLP (mGy-cm)	% $CTDI_{vol}$ Deviation (CD and CTDP)	% $CTDI_{vol}$ Deviation CD and CT Expo	% DLP Deviation (CD and CTDP)	% DLP Deviation CD and CT Expo
AEC	6.94	124.26	6.77	5.3	110.40	166	2.41	23.63	11.15	-33.59
65.00	5.21	93.20	5.11	4.00	83.35	125.00	1.86	23.22	10.57	-34.12
75.00	5.98	107.12	5.89	4.60	95.97	144.00	1.56	23.08	10.41	-34.43
95.00	7.60	136.04	7.48	5.80	121.90	183.00	1.59	23.68	10.39	-34.52
105.00	8.38	149.97	8.28	6.40	135.00	202.00	1.16	23.63	9.98	-34.69

Statistical analysis demonstrated a highly significant correlation between measured and console displayed $CTDI_{vol}$ values ($P < 0.000$, $R^2 = 0.9994$, slope = 0.9952). The high correlation coefficient value (0.9997) suggests that it is reasonable to model the relationship between measured and console displayed $CTDI_{vol}$ values as a linear function as shown in Figure 4.1. The P-values indicate if there is significant difference in the CTDI values between the measured and console displayed. Thus, $P < 0.05$ indicates significant difference and $P > 0.05$ indicates no significant difference between the two CTDI values. The standard error of the mean has a value equal to the length of each arm of the SE bars in mGy. The SEM varies inversely with the square root of the number of samples measured.

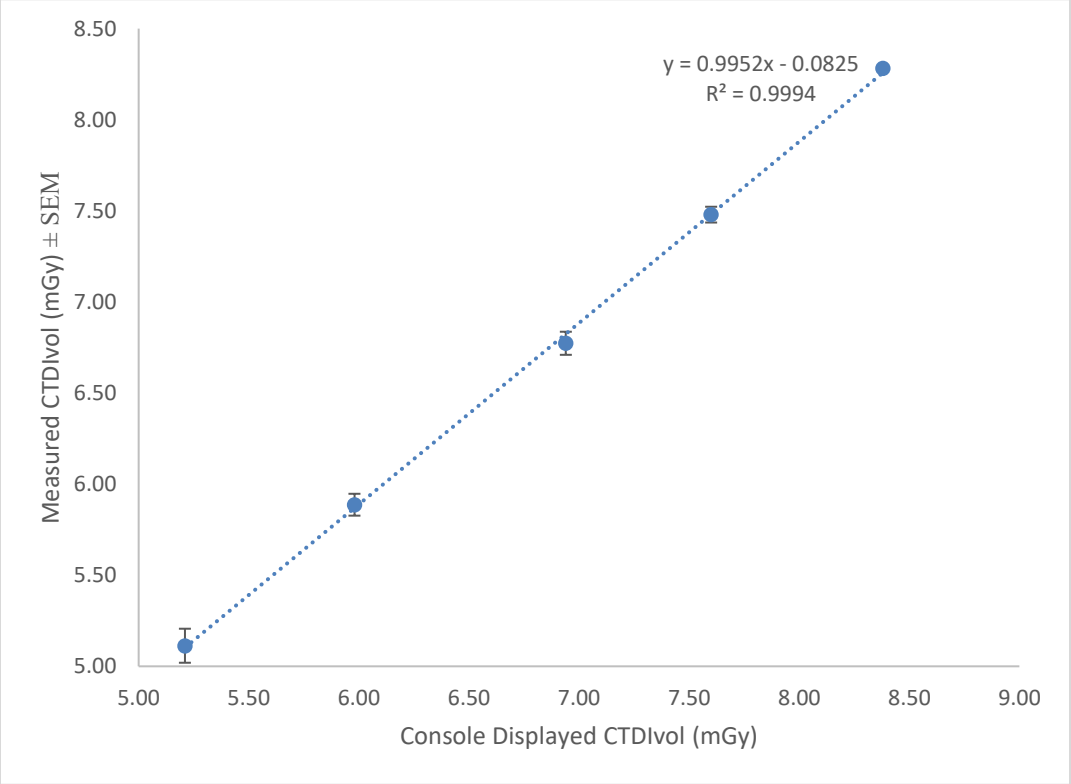

Figure 4. 1: Statistical relation between measured and console displayed $CTDI_{vol}$ values for adult chest exams.

Similar correlation exists between measured and console displayed DLP values ($P < 0.000$, $R^2 = 0.9994$, slope = 0.906) as shown in Figure 4.2.

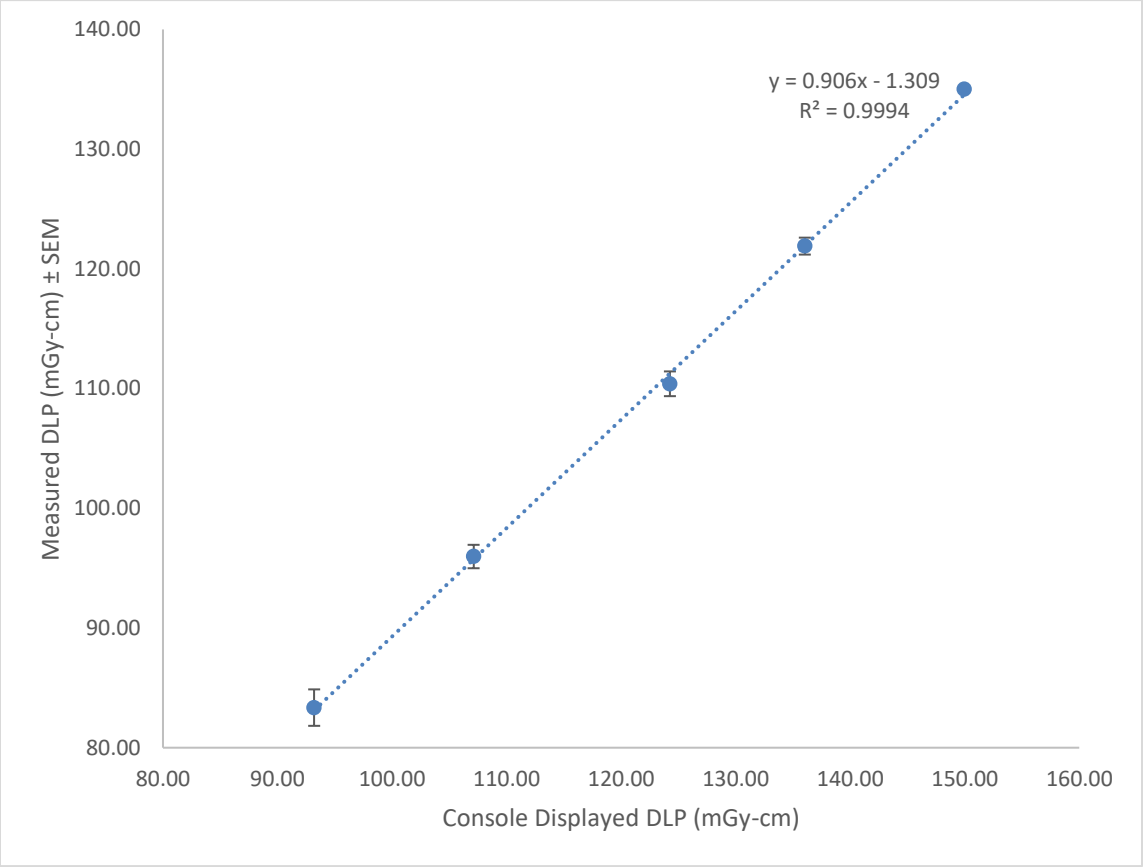

Figure 4. 2: Statistical relation between measured and console displayed DLP values for adult chest exams.

In the same way, the results of $CTDI_{vol}$ and DLP measurements for paediatric chest examinations obtained from the CTDP and that from CT-Expo simulations were compared to the displayed values at the CT console as presented in Table 4.8. From the percent deviations calculated, $CTDI_{vol}$ and DLP values from the CTDP deviated by -68.03 and -

52.83 % and that from CT Expo simulations deviated by -59.47 and -91.55 % respectively from the CT console displayed values.

Table 4. 8: Deviation of measured and simulated $CTDI_{vol}$ and DLP values for paediatric chest CT examination at 110kVp.

Scanning type	**Console Displayed $CTDI_{vol}$ (mGy)**	**Console Displayed DLP (mGy-cm)**	**CTDP $CTDI_{vol}$ (mGy)**	**CT-Expo $CTDI_{vol}$ (mGy)**	**CTDP DLP (mGy-cm)**	**CT-Expo DLP (mGy-cm)**	**% $CTDI_{vol}$ Deviation (CD and CTDP)**	**% $CTDI_{vol}$ Deviation (CD and CT-Expo)**	**% DLP Deviation (CD and CTDP)**	**% DLP Deviation CD and CT-Expo**
AEC	1.68	29.99	2.58	2.70	42.04	58.00	-53.57	-60.71	-40.18	-93.40
16.00	1.32	23.57	-	2.10	-	44.00	-	-59.09	-	-86.68
26.00	2.09	37.49	3.52	3.30	57.25	72.00	-68.42	-57.89	-52.71	-92.05
31.00	2.51	44.99	4.31	4.00	70.20	86.00	-71.71	-59.36	-56.03	-91.15
36.00	2.87	51.42	5.12	4.60	83.50	100.00	-78.40	-60.28	-62.39	-94.48

Note: (-) means no available data

Statistical analysis demonstrated a highly significant correlation between measured and console displayed $CTDI_{vol}$ values ($P < 0.001$, $R^2 = 0.9985$, slope = 2.1068). The high correlation coefficient value (0.9993) suggests that it is reasonable to model the relationship between measured and console displayed $CTDI_{vol}$ values as a linear function as shown in Figure 4.3. The standard error of the mean has a value equal to the length of each arm of the SE bars in mGy.

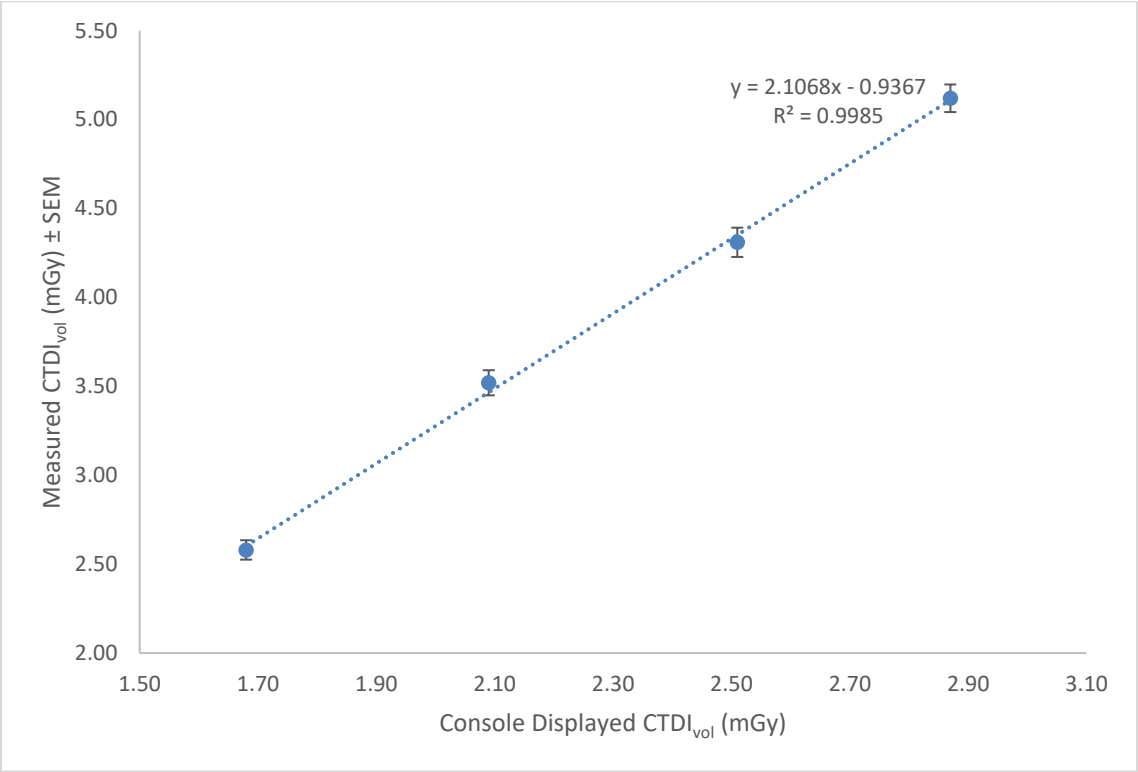

Figure 4. 3: Statistical relation between measured and console displayed $CTDI_{vol}$ values for paediatric chest exams.

Similar correlation exists between measured and console displayed DLP values ($P < 0.001$, $R^2 = 0.9988$, slope = 1.9118) as shown in Figure 4.4.

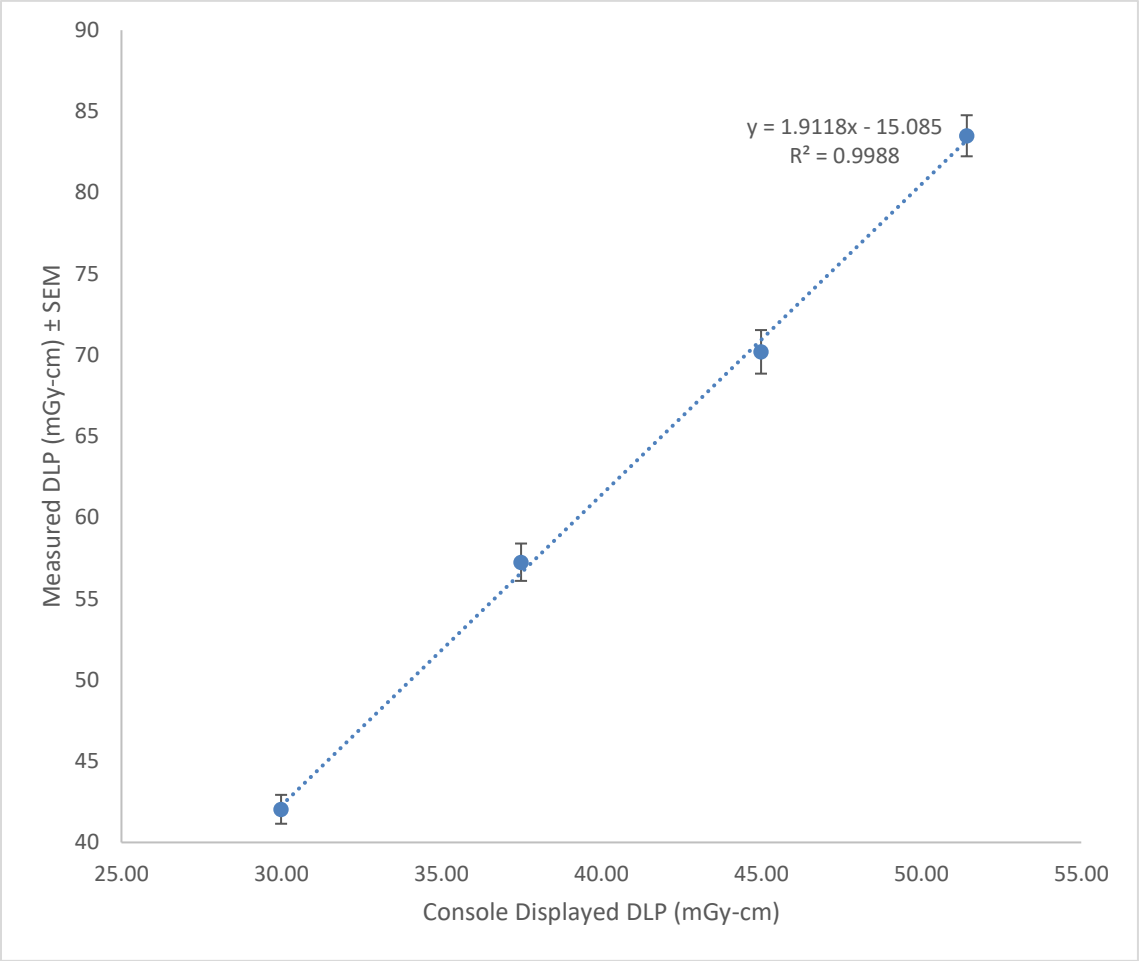

Figure 4. 4: Statistical relation between measured and console displayed DLP values for paediatric chest exams.

4.1.5 Dose Reduction

Estimated dose reduction between the AEC and the FTC techniques for the adult and paediatric chest examinations measurements are presented in Tables 4.9 and 4.10 respectively. There were no significant difference ($p > 0.05$) in the $CTDI_{vol}$ and DLP values between the two techniques.

Table 4. 9: Estimated dose reduction (DR) in $CTDI_{vol}$ and DLP for adult chest CT examination between AEC and FTC techniques.

Scanning type	**$CTDI_{vol}$ (mGy)**	**DR for $CTDI_{vol}$ [%]**	**DLP (mGy-cm)**	**DR for DLP [%]**
AEC	6.77	-	110.40	-
65.00	5.11	-32.47	83.35	-32.45
75.00	5.89	-15.05	95.97	-15.04
95.00	7.48	9.44	121.90	9.43
105.00	8.28	18.23	135.00	18.22
P-value	0.91	-4.96%	0.91	-4.96%

Note: (-) means no available data. The negative sign means no dose reduction.

Table 4. 10: Estimated dose reduction (DR) in $CTDI_{vol}$ and DLP for paediatric chest CT examination between AEC and FTC techniques.

Scanning type	**$CTDI_{vol}$ (mGy)**	**DR for $CTDI_{vol}$ [%]**	**DLP (mGy-cm)**	**DR for DLP [%]**
AEC	2.58	-	42.04	-
26.00	3.52	26.70	57.25	26.57
31.00	4.31	40.14	70.20	40.11
36.00	5.12	49.61	83.50	49.65
P-value	0.06	38.82%	0.06	38.78%

4.1.6 Effective Dose

Effective dose to the chest was calculated using normalised effective dose per dose-length product (DLP) for both adults (standard physique) and paediatric patients based on body weighting factors from ICRP publication 103. The values obtained using CTDP and CT-Expo simulations for adults and paediatric chest CT examinations are presented in Tables

4.11 and 4.12 respectively. Calculated and simulated effective dose values for adult and paediatric chest CT examinations were also compared to values obtained in other similar studies and presented in Tables 4.13 and 4.14.

Table 4. 11: Effective dose values for adult chest CT examination at 110kVp.

Scanning Type	**CTDP E (mSv)**	**CT-Expo E (mSv)**
AEC	1.61	3.60
65.00	1.22	2.70
75.00	1.40	3.10
95.00	1.78	3.90
105.00	1.97	4.40

Table 4. 12: Effective dose values for paediatric chest CT examination at 110kVp.

Scanning Type	**CTDP E (mSv)**	**CT-Expo E (mSv)**
AEC	2.03	1.3
16.00	-	1
26.00	2.76	1.7
31.00	3.38	2
36.00	4.02	2.3

Note: (-) means no available data

Table 4. 13: Comparison of calculated and simulated effective dose values for adult chest CT examinations at 110kVp with other studies.

Study	E (mSv)	
	AEC	FTC
(Breiki et al., 2008) [a]	4.65	-
(Brix et al., 2004) [c]	-	4
(Papadakis., 2011) [a]	2.6	3.07
(Khoramian & Hashemi, 2017) [c]	-	3.45
This study [c]	3.6	3.525(2.7-4.4)
This study [a]	1.61	1.5925(1.22-1.97)

Note: a = Estimated using specific normalized effective dose per DLP conversion factors (k), c = Estimated using Monte Carlo techniques.

Table 4. 14: Comparison of calculated and simulated effective dose values for paediatric chest CT examinations at 110kVp with other studies.

Study	E (mSv)	
	AEC	FTC
(Papadakis et al., 2011) [a]	3.4	3.64
(Brady et al., 2012) [a]	1.8	-
(Galanski et al., 2005) [c]	-	1.3
(Gao et al., 2018) [c]	-	3.4(1.2-5.3)
(Gao et al., 2018) [a]	-	2.2
(Choonik Lee et al., 2007) [c]	-	4.4(3.95-5.45)
(C Lee., 2012) [c]	-	3
This study [c]	1.3	1.75(1-2.3)
This study [a]	2.03	3.39(2.76-4.02)

Note: a = Estimated using specific normalized effective dose per DLP conversion factors (k), c = Estimated using Monte Carlo techniques.

4.1.7 Organ Dose

In Figure 4.5, doses absorbed by the various organs in the adult chest CT examination with AEC and FTC techniques simulated using CT-Expo were compared. The range of radiation dose that resulted from the chest CT examination was 6.2-10 mGy for breast, 5.8-9.4 mGy for lung, 5.9-9.5 mGy for oesophagus and 8.7-14.1 mGy for thyroid. For paediatrics in Figure 4.6, doses absorbed by the various organs in the chest CT examination with AEC and FTC techniques ranged from 2.2-4.9 mGy for breast, 1.9-4.4 mGy for lung, 1.8-4 mGy for oesophagus and 2.2-5 mGy for thyroid.

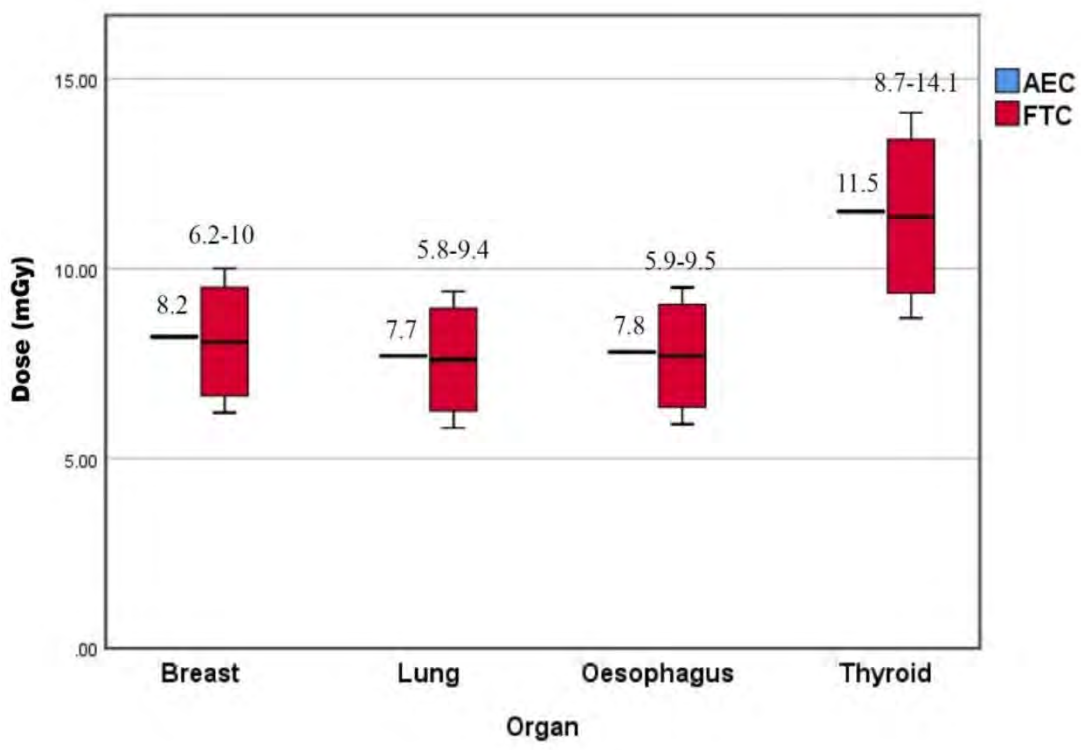

Figure 4. 5: Comparison of adult organ doses for chest CT examinations between AEC and FTC techniques

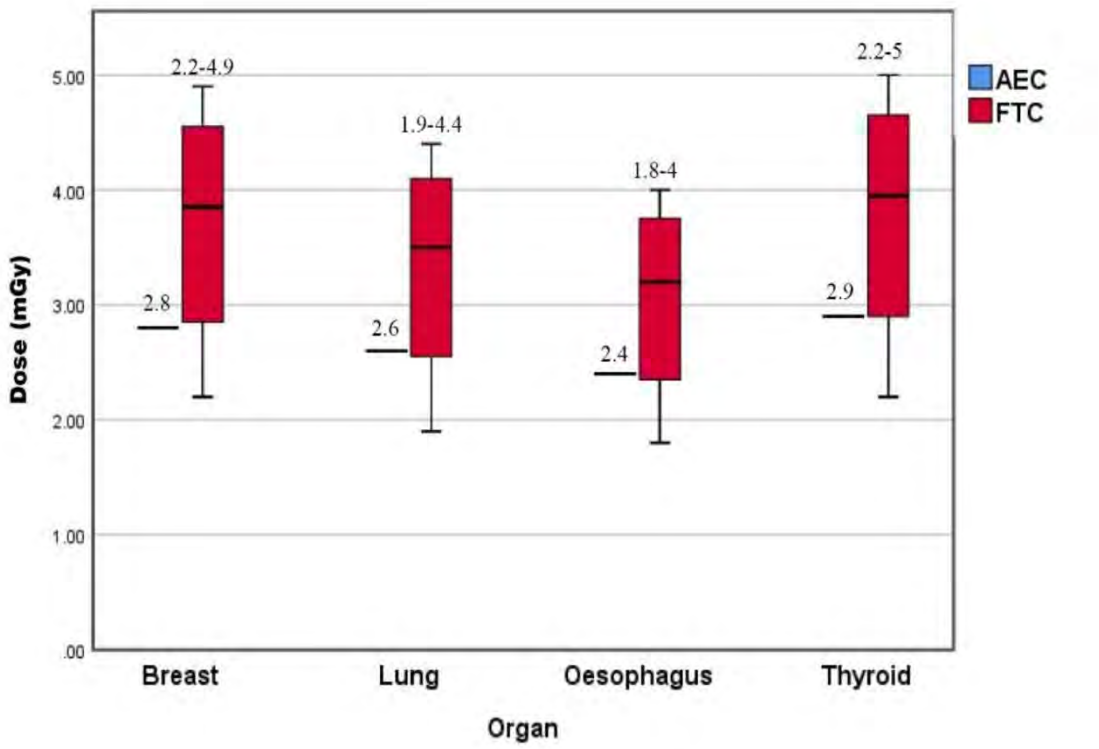

Figure 4. 6: Comparison of paediatric organ doses for chest CT examinations between AEC and FTC techniques.

4.2 Discussions

CTDI is a standardized measure of the radiation dose output of a CT scanner and is used can to compare different scan techniques on a scanner or between scanners. The displayed CTDI values given by a manufacturer may be a representative figure for that model and not the actual value measured on the CT scanner. Absorbed doses measured in this study with the CTDP and estimated doses using CT-Expo simulations were compared to the CT console displayed values. The adults CTDI values measured deviated by 1.71 and 10.50%

for $CTDI_{vol}$ and DLP values respectively which were not so much from the console displayed values compared to that of paediatrics which gave as high deviation in both $CTDI_{vol}$ and DLP values as -68.03 and -52.83% respectively. The simulated CTDI values in paediatrics deviated from the console displayed values with $CTDI_{vol}$ and DLP values of -59.47 and -91.55% respectively and were relatively higher than that of the adults that deviated by 23.40 and -34.44%. A study by Corona et al. (2015) has shown that the DLP values may deviate when the scan length is made a little larger than the head, which affects the DLP calculation by the CT. There are other factors that might have accounted for the outcome as well. For example, considering the findings of Buls et al. (2010) in which reported $CTDI_{vol}$ values from local paediatric scan protocols were compared to measured data with a 16 cm standard dosimetry phantom. They found that for body examinations there has been systematic underestimation of the dose by a median value of 45%. This was attributed to the fact that most users establish paediatric protocols just by downscaling copies of adults. The ratio between the $CTDI_{vol}$ measured in a 16 cm phantom and the $CTDI_{vol}$ measured in a 32 cm phantom is about two even under similar exposure conditions. Thus, a displayed $CTDI_{vol}$ that is calculated for a 32 cm adult phantom underestimates the paediatric radiation dose roughly by a factor of two. This may be a good explanation as routine adult body protocols were downscaled for the paediatric body examinations. Statistical analysis for both adult and paediatric chest CT examinations showed significant difference ($p < 0.05$) between console displayed and measured CTDI values. The slope of the adult $CTDI_{vol}$ curve showed that the measured value increased by 0.9952 times the console displayed value. For the paediatric curve, the measured value increased by 2.1068 times the console displayed value. Similar trend was observed in the DLP curves.

Many CT manufacturers have developed techniques that help reduce radiation dose in CT examinations. Among them is the AEC which has been proven to have dose reduction capability (Sulemana et al., 2018). It is not a good practice to use paediatric modulation settings for adults, and vice versa, because some scanner software packages use distinct modulation curves. This may result in increased dose delivered to children or inadequate doses to adults (Raman et al., 2013) There was no appreciable dose reduction for the adult chest examination (-4.96%) but rather activation of AEC resulted in an increase in dose. For paediatrics, there was a dose reduction of 38.80% estimated between AEC and FTC techniques for both CTDI values. Statistical analysis with paired t-test showed no significant difference between AEC and FTC techniques for both adult and paediatric chest examinations (Tables 4.9-4.10).

Effective dose is an indirect measure of overall radiation detriment owing to stochastic effects and meant for potential dose assessment to enhance planning and optimisation (ICRP, 2007). Unfortunately, no reference dose levels for effective dose given by organizations that deal with radiation levels were obtained for comparison. However, researchers have reported typical (mean) effective dose values from their studies using similar methods. In Table 4.13 calculated and simulated effective dose values for adult chest CT examinations for this study were compared to results of other studies and from the data presented, it is observed that the calculated effective doses for both AEC and FTC techniques were less than the values reported by other researchers by at least 61.49%. However, with CT-Expo simulation, it exceeded that reported by Khoramain and Hashemi (2017) by 2.1 %. Paediatric effective dose values from this study were also compared to results of other studies (Table 4.14). It was noted from the data presented that the calculated effective

doses for both AEC and FTC techniques were greater than other studies (Brady et al., 2012; Gao et al., 2017) except for that reported by Papadakis et al. (2011) which was 67.5 and 7.4% greater for AEC and FTC techniques respectively. For CT-Expo simulation, the estimated effective doses were less than other studies (Gao et al., 2017; Lee et al., 2007; Lee et al., 2012) except for that reported by Galanski et al. (2005) which was 25.7 % less.

To assess risk associated with medical diagnosis in a comprehensive way, it is helpful to study doses to different organs for each CT procedure as opposed to evaluating the effective dose only. It was observed in Figure 4.5 which represented adult chest CT examination that the thyroid had the maximum organ dose ranging from 8.7 to 14.1 mGy for FTC and 11.5 mGy for AEC which lies just above the middle quartile of the FTC technique. For paediatrics as shown in Figure 4.6, the thyroid had the maximum organ dose ranging from 2.2 to 5 mGy for FTC and 2.9 mGy for AEC which lies just above the lower quartile of the FTC techniques. The organ dose levels were, therefore, lower in paediatrics when the AEC technique was used as compared to the FTC technique. This is an indication that the efficacy of the methodology used to capture CT data is challenged in the comparative observation of the different techniques.

The study has some limitations worth discussing. The dose values estimated in this study were based on standard-sized PMMA phantoms and not on human subjects. This could have introduced errors in the dose estimates due to obvious variations in patient sizes from the standard size that the phantoms assume. Nonetheless the dose values can facilitate clinical dosimetry assessment and also serve as a baseline towards establishing optimized dosimetry protocols as these doses can be compared with reference levels to assess the performance of CT scanners. Also, as portrayed by the standard error bars, minimal random

errors where introduced in the dose estimates. The CT-Expo simulations could not represent wider patient ages as it does not include more paediatric phantoms for a wider age rage which could affect the dose calculations. Also, CT-Expo does not offer male breast dose or heart dose to paediatric patients.

CHAPTER FIVE

5.0 CONCLUSION AND RECOMMENDATIONS

5.1 CONCLUSION

Comparison of doses in the study showed that radiation dose delivered to patients may not always be the same as that displayed by the CT console and must not be used for dose estimation and in the establishment of scan protocols. Actual measurement of radiation dose output of a CT scanner must be made with the right phantom size in order to obtain acceptable values consistent with good image quality to prevent overestimation or underestimation of dose. Even though the paediatric doses were relatively high as compared to other studies, there was a dose reduction of 38.80% between the AEC and FTC techniques. The use of AEC has, therefore, proven its efficacy of dose reduction capability particularly in paediatrics as observed even in the organ absorbed doses and lower organ dose levels. Meanwhile, activation of the AEC in the adult chest CT examination resulted in an increase in radiation dose of 4.96% between the AEC and FTC techniques. The use of FTC has therefore shown some level of dose reduction capability that could be used to optimize dose for adults and large patients. In conclusion, both AEC and FTC can be employed in optimization of chest CT examinations and should be incorporated in the establishment of chest CT protocols with respect to patient body size and according to the clinical task.

However, findings from this study, as in many other cited research, support the view that CT scan protocols, especially with paediatric body protocols require more critical consideration. Asking the right questions and estimating the right measurements are

critical, especially for radiation dosages. The study also suggests that scientific techniques such as CT scan also need to be more focused, especially because of the complexity of human nature and the hidden human variations, environmental and unknown previous lifestyles and experiences.

5.2 Recommendations

5.2.1 Further Work by the research community

In modernized CT scan, we see the marriage of digital photography and medical science that would enhance efficient and safe health delivery. It is for this reason that this study considers an approach that would bring both areas together through collaboration and cooperation and crucial considerations consist of improving the balance between dose level and image quality.

1. Further studies should consider using a phantom as close to a patient's disposition including age and sex: VirtualDose is preferable to CT-Expo because it has more paediatric phantoms that can represent broader patient ages, and also uses anatomically realistic phantoms for dose calculations. Also, CT-Expo does not offer male breast dose or heart dose to paediatric patients.
2. A continuation of this work based on the findings should include image quality evaluation to assess the SNR, CNR and spatial resolution to determine the diagnostic relevance of the quality of images produced at such dose levels.
3. Collaborating with the Nuclear Regulatory Administration (NRA), the body responsible for regulating the use of ionizing radiation in Ghana would be an important strategy as it would help establish national diagnostic reference levels.
4. Collaboration with relevant professional bodies and manufacturers would, as well, help to provide the appropriate tools and benchmarks for patient dose optimization in CT

examinations, protocols and facilities. This study indicates that the need for further research cannot be over-emphasized.

5.2.2 Radiographers

Radiographers should particularly consider the use of AEC as a dose reduction technique for patient protection as the technique enables a more accurate and reliable data and for future use.

5.2.3 Sweden Ghana Medical Centre

Management, medical physicists and radiographers at SGMC should consider adopting the methodology used in the establishment of optimized CT scan protocols for both adult and paediatric examinations giving particular attention to paediatrics. Optimization of patient protection should also consider the use of AEC and FTC techniques where appropriate.

REFERENCES

AAPM. (2008). The measurement, reporting, and management of radiation dose in CT. AAPM Report No. 96. Report of AAPM Task Group 23 of the Diagnostic Imaging Council CT Committee.

Ambrose, B. J., & Morley, A. (1973). Computerized transverse axial scanning (tomography): Part 2 . Clinical application *, (December), 1023–1047.

Bauhs, J. A., Vrieze, T. J., Primak, R. T. R. A. N., Bruesewitz, M. R., & Mccollough, R. T. R. C. H. (2008). CT Dosimetry : Comparison of Measure- ment Techniques and devices. *Radiographics*.28(1) : 245–254.

Boone, J. M., Strauss, K. J., Cody, D. D., McCollough, C. H., McNitt-Gray, M. F., Toth, T. L., … Frush, D. P. (2011). AAPM Report No. 204.Size-Specific Dose Estimates (SSDE) in Pediatric and Adult Body CT Examinations. *AAPM Report No. 204*, 1–24. https://doi.org/10.1007/s13398-014-0173-7.2

Brady, Z., Ramanauskas, F., Cain, T. M., & Johnston, P. N. (2012). Assessment of paediatric CT dose indicators for the purpose of optimisation. *British Journal of Radiology*, *85*(1019), 1488–1498. https://doi.org/10.1259/bjr/28015185

Brenner, D. J., Elliston, C. D., Hall, E. J., & Berdon, W. E. (2001). Estimated Risks of Radiation-. *Ajr*, *176*(2), 289–296. https://doi.org/10.2214/ajr.176.2.1760289

Brenner, D. J., & Hall, E. J. (2007). Computed Tomography — An Increasing Source of Radiation Exposure,The new England Journal of Medicince .357: 2277–2284.

Brix, G., Lechel, U., Veit, R., Truckenbrodt, R., Stamm, G., Coppenrath, E. M., … Nagel, H. D. (2004). Assessment of a theoretical formalism for dose estimation in CT: An anthropomorphic phantom study. *European Radiology*, *14*(7), 1275–1284. https://doi.org/10.1007/s00330-004-2267-7

Buls, N., Bosmans, H., Mommaert, C., Malchair, F., Clapuyt, P., & Everarts, P. (2010). CT paediatric doses in Belgium : a multi-centre study, (February).

Butler, P., Morin, R., Creech, W., Dunne, D., Galvin, K., Millette, M., & Frush, D. P. (2016). Image Wisely ® - The US Campaign for Radiation Safety in Adult Medical Imaging, 1–14.

Catalano, C., Francone, M., Ascarelli, A., Mangia, M., Iacucci, I., & Passariello, R. (2007). Optimizing radiation dose and image quality. *European Radiology, Supplement*, *17*(SUPPL. 6), 26–32. https://doi.org/10.1007/s10406-007-0225-6

Chen, G.-P., Noid, G., Tai, A., Liu, F., Lawton, C., Erickson, B., & Li, X. A. (2017). Improving CT quality with optimized image parameters for radiation treatment planning and delivery guidance. *Physics and Imaging in Radiation Oncology*, *4*(October), 6–11. https://doi.org/10.1016/j.phro.2017.10.003

Chen, M. Y. M., Pope, T. L., & Ott, D. J. (2011). *BASIC* (2ND ed.).

College, A. (2008). Acr Practice Guideline for Diagnostic Reference Levels in Medical X-Ray Imaging, 1–6.

Corona, E. C., Ferreira, I. G., & Herrera, J. G. (2015). Verification of CTDI and DLP values for a head tomography reported by the manufacturers of the CT scanners,

using a CT dose profiler probe, a head phantom and a piranha electrometer, ISSSD (2015), 426–435.

Cunningham, I. A., Judy, P. F., & Cunningham, I. A. (2000). Computed Tomography.

Breiki, G., Abbas, Y., El.-Ashry, M., & Diyab, H. (2008). Evaluation of Radiation Dose and Image Quality for Patients Undergoing Computed Tomography (CT) Examinations. *IX Radiation Physics & Protection Conference, Cairo, Egypt*, (November), 15–19.

Galanski, M., Nagel, H. D., & Stamm, G. (2005). Paediatric CT Exposure Practice in the Federal Republic of Germany: Results of a Nation-wide Survey in 2005 / 06. *Mhh*, 56.

Gao, Y., Quinn, B., Pandit-Taskar, N., Behr, G., Mahmood, U., Long, D., … Dauer, L. T. (2018). Patient-specific organ and effective dose estimates in pediatric oncology computed tomography. *Physica Medica*, *45*(August 2017), 146–155. https://doi.org/10.1016/j.ejmp.2017.12.013

Gedel, A. M., & Gablah, P. G. (2014). Management of Radiation Dose to Pediatric Patients undergoing Ct Examination at Korle-Bu Teaching Hospital, Accra – Ghana. *Advances in Physics Theories and Applications, 37(2014)*, 30–38.

Ghetti, C., Ortenzia, O., & Serreli, G. (2012). ORIGINAL PAPER CT iterative reconstruction in image space : A phantom study. *Physica Medica*, *28*(2), 161–165. https://doi.org/10.1016/j.ejmp.2011.03.003

Hall, E. J., & Brenner, D. J. (2008). Cancer risks from diagnostic radiology, *81*(May), 362–378. https://doi.org/10.1259/bjr/01948454

Hatziioannou, K., Papanastassiou, E., Delichas, M., & Bousbouras, P. (2003). A contribution to the establishment of diagnostic reference levels in CT. *British Journal of Radiology*, *76*(908), 541–545. https://doi.org/10.1259/bjr/60897046

Hennequin, R., Abada, H. T., & Chen, X. (2004). Multi – Detector Row Chest CT in Adults : Feasibility and Effect on Image Quality and Iodine Dose 1, (1), 169–174.

Hossain, A. (2015). Polymethyl Methacrylate Phantom on CT Imaging to Evaluate Size-Specific Effective Dose in Pediatric and Adult Body. *International Journal of Biomedical Science and Engineering*, *3*(6), 82. https://doi.org/10.11648/j.ijbse.20150306.13

Hounsfield, G. N. (1973). Computerized transverse axial scanning (tomography): Part I. Description of system, 1016–1022.

International, T. H. E., On, C., & Units, R. (2012). RADIATION DOSE AND IMAGE-QUALITY ASSESSMENT IN COMPUTED, *12*(87).

Jurik, A. G., Jessen, K. A., & Hansen, J. (1997). Image quality and dose in computed tomography. *European Radiology*, *7*(1), 77–81. https://doi.org/10.1007/s003300050114

Kalender, W. A. (2005). CT: The unexpected evolution of an imaging modality. *European Radiology, Supplement*, *15*(4), 21–24. https://doi.org/10.1007/s10406-005-0128-3

Kalra, M. K., Maher, M. M., Toth, T. L., Hamberg, L. M., Blake, M. A., Shepard, J.-A., & Saini, S. (2004). Strategies for CT Radiation Dose Optimization. *Radiology*,

230(3), 619–628. https://doi.org/10.1148/radiol.2303021726

Katada, K. (2002). Characteristics of Multislice CT, *125*(11), 175–179.

Keat, N. (2005). CT scanner automatic exposure control systems, (February).

Khoramian, D., & Hashemi, B. (2017). Effective and organ doses from common CT examinations in one general hospital in Tehran, Iran. *Polish Journal of Medical Physics and Engineering*, *23*(3), 73–79. https://doi.org/10.1515/pjmpe-2017-0013

Kubo, T., Ohno, Y., Ulrich, H., & Hatabu, H. (2014). Radiation dose reduction in chest CT — Review of available options. *European Journal of Radiology*, *83*(10), 1953–1961. https://doi.org/10.1016/j.ejrad.2014.06.033

Kulama, E. (2004). Scanning protocols for multislice CT scanners. *British Journal of Radiology*, *77*(SPEC. ISS.). https://doi.org/10.1259/bjr/28755689

Ledenius, K. (2011). *Optimization of Paediatric CT Examinations An Approach to Minimize Absorbed Dose to Patients with Regard to Image Quality and Observer Variability*. Retrieved from http://hdl.handle.net/2077/24021

Lee, C., Kim, K., Long, D., & Bolch, W. (2012). Organ doses for reference pediatric and adolescent patients undergoing computed tomography estimated by Monte Carlo simulation. *Medical Physics*, *39*(April). Retrieved from http://scitation.aip.org/content/aapm/journal/medphys/39/4/10.1118/1.3693052

Lee, C., Lee, C., Staton, R. J., Hintenlang, D. E., Arreola, M. M., Williams, J. L., & Bolch, W. E. (2007). Organ and effective doses in pediatric patients undergoing helical multislice computed tomography examination. *Medical Physics*, *34*(5),

1858–1873. https://doi.org/10.1118/1.2723885

Lewis, M. a, & Edyvean, S. (2005). Patient dose reduction in CT. *The British Journal of Radiology*, *78*(934), 880–883. https://doi.org/10.1259/bjr/75960844

Livingstone, R., Pradip, J., Dinakran, P., & Srikanth, B. (2010). Radiation doses during chest examinations using dose modulation techniques in multislice CT scanner. *Indian Journal of Radiology and Imaging*, *20*(2), 154. https://doi.org/10.4103/0971-3026.63036

McCollough, C. H., Primak, A. N., Braun, N., Kofler, J., Yu, L., & Christner, J. (2009). Strategies for Reducing Radiation Dose in CT. *Radiologic Clinics of North America*, *47*(1), 27–40. https://doi.org/10.1016/j.rcl.2008.10.006

Mccollough, C. H., & Zink, F. E. (1999). Performance evaluation of a multi-slice CT system Performance evaluation of a multi-slice CT system a …, *2223*(1999). https://doi.org/10.1118/1.598777

Monty W. Charles; ICRP Publication 103: Recommendations of the ICRP, Radiation Protection Dosimetry, Volume 129, Issue 4, 1 May 2008, Pages 500–507, https://doi.org/10.1093/rpd/ncn187

Muhogora, W. E., Ahmed, N. A., Beganovic, A., Benider, A., Ciraj-Bjelac, O., Gershan, V., … Rehani, M. M. (2009). Patient doses in CT Examinations in 18 countries: Initial results from international atomic energy agency projects. *Radiation Protection Dosimetry*, *136*(2), 118–126. https://doi.org/10.1093/rpd/ncp144

Papadakis, A. E., Perisinakis, K., & Damilakis, J. (2008). Automatic exposure control in

pediatric and adult multidetector CT examinations : A phantom study on dose reduction and image quality. *Medical Physics,* 35(10) : 4567–4576. https://doi.org/10.1118/1.2977535

Papadakis, A. E., Perisinakis, K., Oikonomou, I., & Damilakis, J. (2011). Automatic Exposure Control in Pediatric and Adult Computed Tomography Examinations. *Investigative Radiology*, *46*(10), 654–662. https://doi.org/10.1097/RLI.0b013e3182213c55

Paterson, A., Frush, D. P., & Donnelly, L. F. (2001). Helical CT of the Body: *Pediatric Radiology*, (February), 297–301. https://doi.org/10.2214/ajr.176.2.1760297

Pearce, M. S., Salotti, J. A., Little, M. P., Mchugh, K., Lee, C., Kim, K. P., … Victoria, R. (1985). Radiation exposure from CT scans in childhood and subsequent risk of leukaemia and brain tumours : a retrospective cohort study. *The Lancet*, *380*(9840), 499–505. https://doi.org/10.1016/S0140-6736(12)60815-0

Primak, A. N., McCollough, C. H., Bruesewitz, M. R., Zhang, J., & Fletcher, J. G. (2006). Relationship between Noise, Dose, and Pitch in Cardiac Multi–Detector Row CT. *RadioGraphics*, *26*(6), 1785–1794. https://doi.org/10.1148/rg.266065063

Raman, S. P., Mahesh, M., Blasko, R. V., & Fishman, E. K. (2013). CT scan parameters and radiation dose: Practical advice for radiologists. *Journal of the American College of Radiology*, *10*(11), 840–846. https://doi.org/10.1016/j.jacr.2013.05.032

Shope, T. B., Gagne, R. M., & Johnson, G. C. (1981). A method for describing the doses delivered by transmission xÃ¢â‚¬Â•ra y computed tomography. *Medical Physics*,

8(4), 488–495. https://doi.org/10.1118/1.594995

Siegel, M. J., Schmidt, B., Bradley, D., Suess, C., & Hildebolt, C. (2004). Radiation Dose and Image Quality in Pediatric CT: Effect of Technical Factors and Phantom Size and Shape. *Radiology*, *233*(2), 515–522. https://doi.org/10.1148/radiol.2332032107

Söderberg, M., & Gunnarsson, M. (2010). Acta Radiologica manufacturers. https://doi.org/10.3109/02841851003698206

Sookpeng, S., Martin, C. J., & Gentle, D. J. (2013). A Study of Dose Distribution and Image Quality under an Automatic Tube Current Modulation (ATCM) System for a Toshiba Aquilion 64 CT Scanner Using a New Design of Phantom, International Journal of Medical, Health, Biomedical, Bioengineering and Pharmaceutical Engineering.*44*(1): 1–7.

Stamm, G., & Nagel, H. D. (2017). CT-Expo v2.5, (February).

Suess, C. (2002). Dose optimization in pediatric CT : current technology and future innovations, 729–734. https://doi.org/10.1007/s00247-002-0800-x

Sulemana, H., Inkoom, S., Schandorf, C., Sosu, E., & Kaka, D. Y. (2018). Assessment of Adult Patient Radiation Dose and Image Quality in CT Examinations Performed Using Automatic Exposure Control and Fixed Tube Current Techniques : A Phantom Case Study, *4*(5), 1285–1289.

Szucs-farkas, Z., Kurmann, L., Strautz, T., Patak, M. A., Vock, P., & Schindera, S. T. (2008). Patient Exposure and Image Quality of Low-Dose Pulmonary Computed Tomography Angiography, *43*(12), 871–876.

Trattner, S., Pearson, G. D. N., Chin, C., & Cody, D. D. (2014). Standardization and Optimization of CT Protocols to Achieve Low Dose. *Journal of the American College of Radiology*, *11*(3), 271–278. https://doi.org/10.1016/j.jacr.2013.10.016

UNSCEAR. (2008). *SOURCES AND EFFECTS United Nations Scientific Committee on the Effects of Atomic Radiation* (Vol. I).

Weber, A. L. (2001). Reflections History of Head and Neck Radiology : Past , Present , and Future 1, *1901*(4), 15–24.

Yu, L., Li, H., Fletcher, J. G., Mccollough, C. H., Yu, L., Li, H., … Mccollough, C. H. (2010). Automatic selection of tube potential for radiation dose reduction in CT : A general strategy Automatic selection of tube potential for radiation dose reduction in CT : A general strategy, *234*. https://doi.org/10.1118/1.3264614

Zenger, I. (2015). The History of Computed Tomography at Siemens A retrospective, 1–55.

Zink, F. E. (1997). X-ray tubes. *Radiographics : A Review Publication of the Radiological Society of North America, Inc*, *17*(5), 1259–1268. https://doi.org/10.1148/radiographics.17.5.9308113